104 (2025) 104995

Contents lists available at ScienceDirect

Poultry Science

journal homepage: www.elsevier.com/locate/psj

Single-cell RNA sequencing of bone marrow reveals the immune response mechanisms of lymphocytes under avian leukosis virus subgroup J infection

Cheng Liu [a,1], Yu Zhang [a,1], Ruyu Liao [a], Lecheng Wang [a], Xinyi Zhou [a], Min Tan [a], Keyun Xu [a], Haiwei Wang [b], Qigui Wang [b], Yongju Zhao [a], Zhifu Cui [a,**], Xi Lan [a,*]

[a] College of Animal Science and Technology, Southwest University, Chongqing 400715, China
[b] Chongqing Academy of Animal Science, Chongqing, China

ARTICLE INFO

Keywords:
ALV-J
scRNA-seq
Bone marrow
Lymphocytes
Immune suppression

ABSTRACT

Avian Leukosis Virus (ALV) can induce tumorigenesis and immune suppression by acting on lymphocytes in the bone marrow. In this study, single-cell RNA sequencing (scRNA-seq) was used to analyze chicken bone marrow lymphocytes under Avian Leukosis Virus subtype J (ALV-J) infection. Using subgroup-specific marker genes and cell state analysis, we identified 18 distinct cell clusters, including 8 T cell clusters, 2 B cell clusters, 5 tumor-like cell clusters, and 3 unidentified clusters. Gene expression analysis revealed that in the 10 T/B lymphocyte clusters, the differentially expressed genes in double-positive T cells, B1-like B cells, and cytotoxic T cells were highly enriched in pathways related to viral infection and immune response. These three cell populations exhibited high proportions and significant changes after infection, suggesting a strong immune response to ALV-J infection. Additionally, during ALV-J infection, the proportion of regulatory T cells and *CTLA4* T cells increased, while immune suppressive factors *TGFB1* and *IL16* were highly expressed across the cell populations, indicating an immune-suppressive state in bone marrow lymphocytes. Moreover, ALV-J infected all cell populations; however, within the same cluster, only a fraction of the cells expressed ALV-J viral genes. Notably, in all cells expressing ALV-J viral genes, the "Rho family GTPase signaling pathway" associated with antiviral responses was activated. The Rho family, which is a key regulator of cytoskeletal reorganization and cell polarity, also plays a critical role in tumor cell proliferation and metastasis. Further analysis using Ingenuity Pathway Analysis (IPA) software predicted key upstream regulators of immune response, such as *MYC* and *MCYN*. In conclusion, this study identifies key genes and signaling pathways involved in immune responses of different lymphocyte subpopulations triggered by ALV-J infection in bone marrow. These findings contribute to a better understanding of the immune mechanisms in ALV-J-infected bone marrow lymphocytes and provide insights for discovering breeding loci for ALV-J resistance.

Introduction

Avian Leukosis Virus (**ALV**) is a retrovirus that induces various leukemia-like tumor diseases. ALV is classified into 11 subtypes, labeled A–K, among which Avian Leukosis Virus subtype J (**ALV-J**) has caused significant losses to the global poultry industry due to its high transmissibility and pathogenicity (Payne and Nair, 2012). However, there is currently no effective vaccine or drug available for this disease. Since ALV-J was first isolated from broiler chickens in the United Kingdom (Payne et al., 1991), it has been regarded as a virus that induces leukemia in bone marrow cells. In 2003, field cases of myelogenous leukemia caused by ALV-J in commercial egg-laying hens were first reported (Xu et al., 2004). Studies have shown that ALV-J induces myelogenous leukemia in hosts, primarily through myeloproliferative disorders, myeloma, and hemangioma (Lai et al., 2011; Payne and Nair, 2012). Myelogenous leukemia is a disease caused by the malignant proliferation of hematopoietic stem cells or their differentiated cells, where hematopoietic stem cells differentiate into lymphocytes and myeloid cells in the bone marrow. Increasing evidence suggests that immune cell dysfunction in the bone marrow is closely linked to

* Corresponding author at: No. 2 Tiansheng Road, College of Animal Science and Technology, Southwest University, Chongqing 400715, China.
** Corresponding authors.
E-mail addresses: cui20221732@swu.edu.cn (Z. Cui), xlan104@swu.edu.cn (X. Lan).
[1] These two authors are co-first authors.

https://doi.org/10.1016/j.psj.2025.104995
Received 7 December 2024; Accepted 5 March 2025
Available online 8 March 2025

leukemia (Epling-Burnette and List, 2009; Glenthøj et al., 2016). In addition to causing leukemia, ALV-J infection also leads to immune suppression. ALV not only inhibits the differentiation and maturation of bone marrow-derived dendritic cells and induces apoptosis but also causes apoptosis of monocytes (Dai et al., 2017; Liu et al., 2016a, b). However, research on how ALV-J induces lymphocyte immune suppression is limited. Current studies have found that in viruses causing immune suppression, the proportion of regulatory T cells increases in patients infected with Hepatitis B Virus (**HBV**), along with a rise in exhausted T cells (Duan et al., 2018; Ho et al., 2021). When infected with Influenza A Virus (**IAV**), the body produces cytokines such as *CCl3, CCl4*, and *TNF-α* to combat the virus (Ho et al., 2021). Therefore, it is crucial to study the status of lymphocytes in bone marrow under ALV-J infection.

The maturation of single-cell sequencing technology has greatly facilitated research on highly heterogeneous immune cells. Single-cell RNA sequencing (**scRNA-seq**) has been used to monitor the composition and functional status of T cells in the tumor microenvironment of non-small cell lung cancer patients (Li et al., 2020), as well as to reveal the suppressive tumor microenvironment in human colorectal cancer (Mei et al., 2021). It has also been used in combination with extensive RNA-seq analyses to reveal dynamic changes in the tumor immune microenvironment and to establish prognostic models (Chen et al., 2022; Fang et al., 2022; Tan et al., 2023). In recent years, scRNA-seq technology has made significant progress in animal and poultry research. In studies on cattle, scRNA-seq has been primarily applied to explore areas related to production performance, such as bovine skeletal muscle, adipose tissue, and embryo cells (Cai et al., 2023; Wang et al., 2023a, b). Similarly, research on sheep also focuses on production performance-related fields (Ge et al., 2023; Hu et al., 2021; Yang et al., 2021). In chickens, single-cell sequencing studies have not only addressed production performance but have also explored mechanisms related to poultry disease immunity (Li et al., 2020), such as the potential mechanisms underlying avian influenza virus (**AIV**)-induced inflammatory responses in chickens (Dai et al., 2023), as well as the response of chicken peripheral blood mononuclear cells during viral infections (Qu et al., 2022). Although research on the avian immune system has been ongoing for decades, most knowledge of avian lymphocytes has been derived from mammals (such as humans and mice), and there is still limited understanding of the unique characteristics of avian lymphocytes (Dai et al., 2019a). To date, there has been no study using scRNA-seq technology to investigate the lymphocyte immune response in the bone marrow of chickens infected with ALV-J.

In this study, we collected bone marrow lymphocytes from chickens in an ALV-J infection state and used 10x scRNA-seq technology for comprehensive identification and characterization. The results showed that, under ALV-J infection, double-positive T cells, B1-like B cells, and cytotoxic T cells in the bone marrow were closely related to viral infection and immune responses. Additionally, the immune suppression induced by ALV-J infection may be linked to *TGFB1, IL16, CTLA4* T cells, and regulatory T cells. Notably, when exposed to ALV-J virus infection, there were differences in susceptibility among different cell populations, and even within the same population, cells showed varying levels of susceptibility to ALV-J. However, in all cells expressing ALV-J genes, the "Rho family GTPase signaling pathway," which is closely associated with tumor cell development and progression, was activated. Further analysis using IPA software revealed that ALV-J infection significantly impacted the marker genes and functions of both known and unknown immune cells in chickens.

Materials and methods

Chickens

In this experiment, four 500-day-old Nanchuan chickens (a local Chinese breed) were utilized, including two infected with ALV-J and exhibiting tumor tissues as the avian leukosis virus infection group, and two without tumor tissues as the control group. To ensure accurate grouping, the chickens were first tested for ALV-J infection using ALV-J specific primers. Subsequently, an ALV-J specific P27 ELISA antigen detection kit (NEVCB, China) was employed to determine whether the chickens were persistently shedding the virus and whether viremia was present. The ALV-J specific antibody kit (IDEXX, USA) was used to determine the serum ALV-J antibody in chickens. The chickens with PCR positive, continuous cloacal detoxification, positive viremia, and positive antibodies were named as ALV, and the chickens with PCR positive, no cloacal detoxification, negative viremia, and positive antibodies were named as NC. Autopsy revealed remarkable tumor tissue visible in the liver of two chickens in sample ALV, whereas sample NC did not show any (Figure S1). By using Marek's disease virus (**MDV**) and reticuloendotheliosis virus (**REV**) specific primers, the chickens were found to be not infected with these two tumorigenic viruses. All test results are shown in Figure S1, and detailed primer information is provided in Table S2.

RNA extraction and quantitative real-time polymerase chain reaction (qRT-PCR)

Total RNA was extracted from the bone marrow by using TRIzol reagent (Invitrogen, Carlsbad, CA, USA) in accordance with the manufacturer's guide and then reversely transcribed into cDNA by using a reverse transcription kit (TaKaRa, Tokyo, Japan). qRT-PCR was carried out to detect the mRNA expression by utilizing SYBR Premix Ex TaqTM (TaKaRa) on Bio-RAD (USA) following the protocols. The relative expression was calculated utilizing the 2-ΔΔCt method. All primers involved are listed in the Table S2.

Preparation of bone marrow lymphocyte single-cell suspension

Considering that flow cytometry-based isolation of chicken lymphocytes could be affected by cell phenotype, reagents, and progenitor T cells in the bone marrow (Dai et al., 2019b), chicken lymphocyte isolate (Solarbio, China) was chosen for this experiment to more adequately isolate lymphocytes from the bone marrow. The brief steps are as follows: first, the obtained chicken tibia was immediately placed in pre-cooled PBS. Second, the epiphyses at both ends were removed, and the bone marrow tissue was gently pulled out with forceps. Next, the bone marrow tissue was cut up and added to three times the volume of collagenase I (1 mg/mL and digested at 37 °C for 25 min and then two times the volume of DMEM to terminate the digestion. The digest was rapidly passed through a 40 μm cell sieve and centrifuged at 2000 rpm/min for 5 min. Subsequently, the precipitate was resuspended, and the resuspension was gently added to the top of the lymphatic isolate and centrifuged at 1700 rpm/min for 25 min. Then, the lymphocytes were aspirated, and 10 mL of PBS was aspirated and blown softly. Afterwards, centrifugation was conducted at 1000 rpm/min for 10 min, the precipitate was resuspended, and the cell concentration was adjusted to 1000–2000 cells/μl. Cell activity was determined by placental blue staining microscopy, and cell viability greater than 80 % was used for single-cell library construction.

Single-cell library construction

Chromium Single Cell 3′ Gel Bead in Emulsion (**GEM**) Library and Gel Bead Kit were used to barcode cell suspensions and reverse-transcribed into scRNA-seq libraries in accordance with the manufacturer's instructions. In brief, the obtained chicken bone marrow lymphocytes were individually barcoded, labeled, and mixed with reverse transcriptase into GEM. cDNA libraries were constructed using sequencing primers R1 and R2, followed by ligation of P5 and P7 Illumina sequencing connectors. Finally, the cDNA library was sequenced on the Illumina 10x Genomics Chromium platform (Illumina Novaseq 6000).

Data processing

Alignment of reads to the chicken reference genome [*Gallus gallus* (chicken), GCA_000002315.5] was performed using Cell Ranger by calling Spliced Transcripts Alignment to a Reference (**STAR**) alignment software. Only reads that were sufficiently mapped to the transcriptome database were used for unique molecular identifier (**UMI**) counting. By using the R package Seurat to filter multicell and null cell data, cells with $>$ 8000 genes or $<$ 200 genes, $>$ 5000 UMIs, and $>$ 25 % mitochondrial gene expression ratio were filtered out. The data were homogenized by log homogenization with the use of ScaleData to correct for differences in library size and the number of mitochondrial UMIs.

Dimensionality reduction and visualization

In accordance with the jackstraw procedure (Levine et al., 2015), the first 50 principal components were used for downstream clustering and dimensionality reduction. Subsequently, graph-based clustering was implemented using Seurat (Becht et al., 2019). Visualization and data analysis were carried out using uniform manifold approximation and projection (**UMAP**) (Trapnell et al., 2014).

Analysis of upregulated differentially expressed genes (DEGs) in various subgroups

Seurat's rank sum test was used for DEG analysis of individual cell subpopulations relative to all other cell subpopulations. The genes were screened for differential upregulation in each cell subpopulation on the basis of the following conditions: log2FC $\geq$ 0.36 (log2FC indicates the fold change in expression values between comparison groups after logging); $P \leq 0.01$; and the gene was expressed in more than 25 % of cells in the target subpopulation. Subsequently, Pearson's correlation analysis was performed to investigate the correlation between different subgroups on the basis of gene expression levels. The DEGs were mapped to each term of the Gene Ontology (**GO**) database (http://www.geneontology.org/), and the number of genes per term was counted to obtain a list of genes with a particular GO function and a count of the number of genes. Then, hypergeometric test was applied to identify GO terms that were significantly enriched in DEGs compared to the whole background. Pathway significant enrichment analysis was performed using Kyoto Encyclopedia of Genes and Genomes (**KEGG**), and hypergeometric test was also applied to identify pathways that were significantly enriched in DEGs compared to the background genes.

Receptor-ligand analysis

CellChat V2.1.0 software can use the gene expression matrix of single cells to analyze the communication ligand-receptor pairs between cell subpopulations and their expression information, and construct the interaction network diagram of cells at the level of ligand receptors, so as to predict the potential communication network relationship between cells.

The gene expression matrix and cell grouping information of single cells were input, and the pairing information of ligand contained in the CellChatDB database was used to analyze the communication intensity of each pair of cells based on the way that one cell expressed the receptor and the other cell expressed the ligand. The statistical test value Pvalue of the communication probability of each mating acceptor was calculated by the method of substitution test, and $P < 0.05$ was used as the retention threshold for filtering according to the statistical significance. The unfiltered information is also provided in the attachment, with the suffix all.

Gene set variance analysis (GSVA)

GSVA is a non-parametric unsupervised analysis method mainly used to evaluate the gene set enrichment results of sequencing. The expression matrices of genes are transformed into expression matrices of pathways in different subgroups to assess the different metabolic pathways enriched in different subgroups. In this study, GSVA was performed using the GSVA package in R software, and then the immune-associated gene set c7. immunesigdb_HALLMARK was used.

Pseudotime analysis

The expression matrix of cells and genes in Monocle 2 was used to map the differentiation trajectories of single cells (Szklarczyk et al., 2015). Monocle reduces the space in which cells are embedded to two dimensions and sorts the cells (parameters: sigma = 0.001, lambda = NULL, param. $\gamma = 10$, and tol = 0.001). Once the cells are sorted, trajectories (with a tree-like structure, including tips and branches) could be visualized in the reduced dimensional space.

Viral load analysis

Cellular infection with ALV-J was determined by the number of UMI fragments of ALV-J. In brief, to exclude false positives, the number of UMIs matching on the ALV-J strain, defined as 0.01 % of the total number of UMIs, was defined as infected cells. Therefore, 0 %–0.01 %, 0.01 %–0.1 %, 0.1 %–0.5 %, and 0.5 % or more were defined as no-viral-load cells, low-viral-load cells, medium-viral-load cells, and high-viral-load cells, respectively.

Ingenuity pathway analysis (IPA)

IPA was used to discover relevant modulate pathways and transcriptional network in accordance with Fisher's exact test enrichment statistics and Benjamini–Hochberg corrected *P*-value calculations. In non-model species, the minimum number of genes recommended by IPA is 200. The DEGs were uploaded for IPA analysis between cells with and without viral load from the same cell subpopulation, which included cluster_0, cluster_1, cluster_3, cluster_4, cluster_5, cluster_6, cluster_8, cluster_10, cluster_11, cluster_12, cluster_14, and cluster_15. The DEGs between samples in cluster_7 and the upregulated DEGs in cluster_7_1 were also uploaded for IPA analysis.

Analysis of DEGs between samples for each cluster

The DEGs of each subpopulation between sample ALV and sample NC were analyzed using Seurat to explore the response of bone marrow lymphocytes in different infection states. The DEGs were identified by the following conditions: $|\log2FC| \geq 1$, $P \leq 0.01$, and proportion of genes in a specific subpopulation $>$ 25 %. The DEGs were then analyzed for GO and KEGG as described above. Gene set enrichment analysis (**GSEA**) was performed using the desktop tool from http://software.broadinstitute.org/gsea/index. In addition, GSVA analysis was performed on the dataset.

Immunohistochemistry

Dewaxed and hydrated bone marrow slides were placed in the antigen repair solution and boiled for 20 min. Then, the slides were blocked with 5 % BSA for 30 min at ambient temperature. Next, the slides were incubated with anti-Bu-1 mouse monoclonal antibody and anti-CD4 rabbit monoclonal antibody overnight at 4 °C. Afterwards, they were incubated with biotin-labeled secondary antibodies for 1 h at ambient temperature, followed by color development with DAB. Finally, the slides were counterstained with hematoxylin. The magnification of the immunohistochemistry images was 100 $\times$.

Protein–protein interaction (PPI) network

STRING (version 10.0) and Cytoscape (version 3.3.0) software were used to construct interaction maps of candidate differential genes. Specifically, the PPI network was constructed using STRING (Shannon et al., 2003), which identifies genes as nodes and interactions as lines in the network. The constructed network was visualized using Cytoscape software (Visco et al., 2020b) to present the interactions between core genes.

Results

ScRNA-seq obtained eighteen clusters

In this study, lymphocytes isolated from chicken tibial bone marrow were subjected to 10x single-cell RNA sequencing. The transcriptional features of all captured cells are shown in Fig. 1A. After quality control, a total of 30,137 valid cells were obtained, including 7,746 cells in the NC1 sample, 7,802 cells in the NC2 sample, 8,115 cells in the ALV1 sample, and 6,474 cells in the ALV2 sample. Graph-based clustering analysis was performed using UMAP to group cells with similar expression profiles together. By performing dimensionality reduction and unsupervised clustering through UMAP, a total of 18 distinct cell clusters were identified (Fig. 1B and C). Among these, nine clusters were more abundant in the NC samples than in the ALV samples, including Cluster_0, Cluster_1, Cluster_3, Cluster_4, Cluster_5, Cluster_8, Cluster_12, Cluster_13, and Cluster_17 (Fig. 1D). Additionally, ten clusters were highly expressed in both sample groups, including Cluster_0, Cluster_1, Cluster_2, Cluster_3, Cluster_4, Cluster_5, Cluster_6, Cluster_7, Cluster_8, and Cluster_9 (Fig. 1E). To identify the marker genes for the 18 subpopulations, we calculated the differentially upregulated genes for each subpopulation relative to others and selected the top five genes as markers for each group (Fig. 1F). In subsequent studies, we identified 10 lymphocyte subpopulations (Cluster_2, Cluster_7, Cluster_8, Cluster_9, Cluster_10, Cluster_13, Cluster_14, Cluster_15, Cluster_16, Cluster_17). The proportion of lymphocytes in the ALV group was approximately 52.73 %, while in the NC group, it was approximately 14.94 %. The proportion of lymphocytes was significantly higher in the ALV samples compared to the NC samples (Table S6).

Two B cell clusters and eight T cell clusters were identified

Lymphocyte subpopulations were identified using lymphocyte-specific marker genes. Cluster_7 and Cluster_8 expressed the B cell-specific marker gene *CD79B* (Visco et al., 2020a) (Fig. 2A and B) and also highly expressed *BLB2* (Potts et al., 2019) and *Basp1* (Medaglia et al., 2017) (Fig. 2A). Cluster_7 specifically highly expressed *BHLHE41*, a gene related to B1 cell development (Kreslavsky et al., 2017) (Fig. 2A), and the chicken B cell-specific marker gene *Bu-1* (Pal et al., 2020) (Fig. 2A and B). Thus, Cluster_7 was classified as a B1-like B cell cluster. Cluster_8 expressed antibody-related genes *JCHAIN, IGLC1*, and *IGHA1* (Castro and Flajnik, 2014; Ye et al., 2021), as well as the B2 cell-related gene *CCR10* (Xiong et al., 2012) (Fig. 1F), thus it was classified as a plasma cell-like cluster.

In the T cells, based on the T cell-specific marker gene *CD3D*, eight T cell clusters were identified: Cluster_2, Cluster_9, Cluster_10, Cluster_13, Cluster_14, Cluster_15, Cluster_16, and Cluster_17 (Fig. 2C). Cluster_2 expressed both *CD8A* and *CD4*, thus it was classified as a CD8+CD4+ *T* cell cluster (Fig. 2B and D). CD8+CD4+ *T* cells are also referred to as double-positive T cells, CD8+CD4+ *T* cells are also known as double-positive T cells. Cluster_9 highly expressed *CD8A* and the cytotoxicity-related genes *GNLY, GZMA*, and *FAS* (Fig. 2B and D), and thus was classified as a cytotoxic T cell cluster. Although Cluster_16 expressed *CD4* at low levels (Fig. 2D), it highly expressed Th2-related genes *KK34* (Koskela et al., 2004) and *DRD4* (Wang et al., 2019) (Fig. 2C), and also expressed *TGFB1* (Fig. 2D). Recent studies have identified a new class of

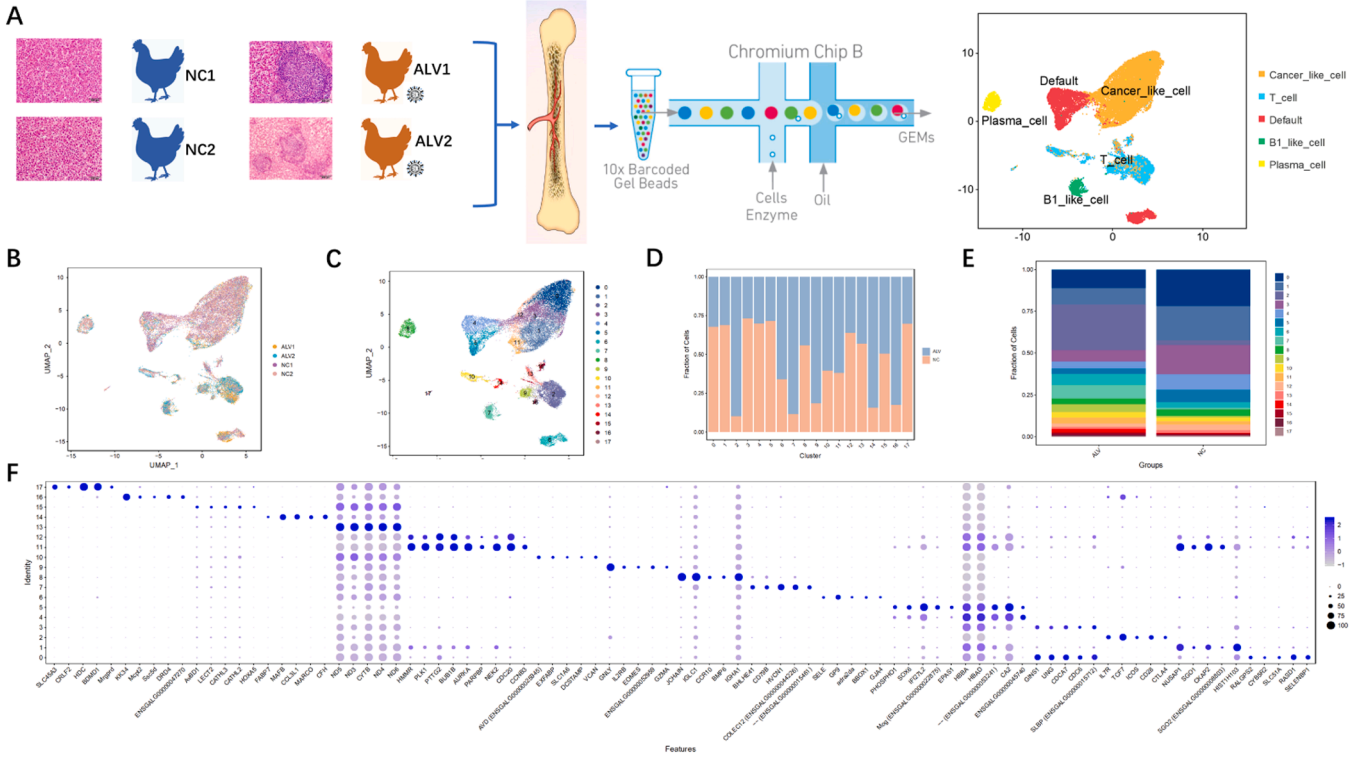

Fig. 1. ***ScRNA-seq obtained eighteen clusters.*** A: Overview of the study design. The bone marrows of four chickens infected with ALV-J in different states were collected, the lymphocytes were separated from the bone marrow, and then single-cell sequencing analysis was conducted. B and C: UMAP display of all cell populations in samples ALV and NC. D and E: Proportion of each cluster in the sample ALV and NC. F: Top five DEGs identified in each cluster. Dot size represents the proportion of cells in the cluster that expresses the gene; intensity indicates the mean expression.

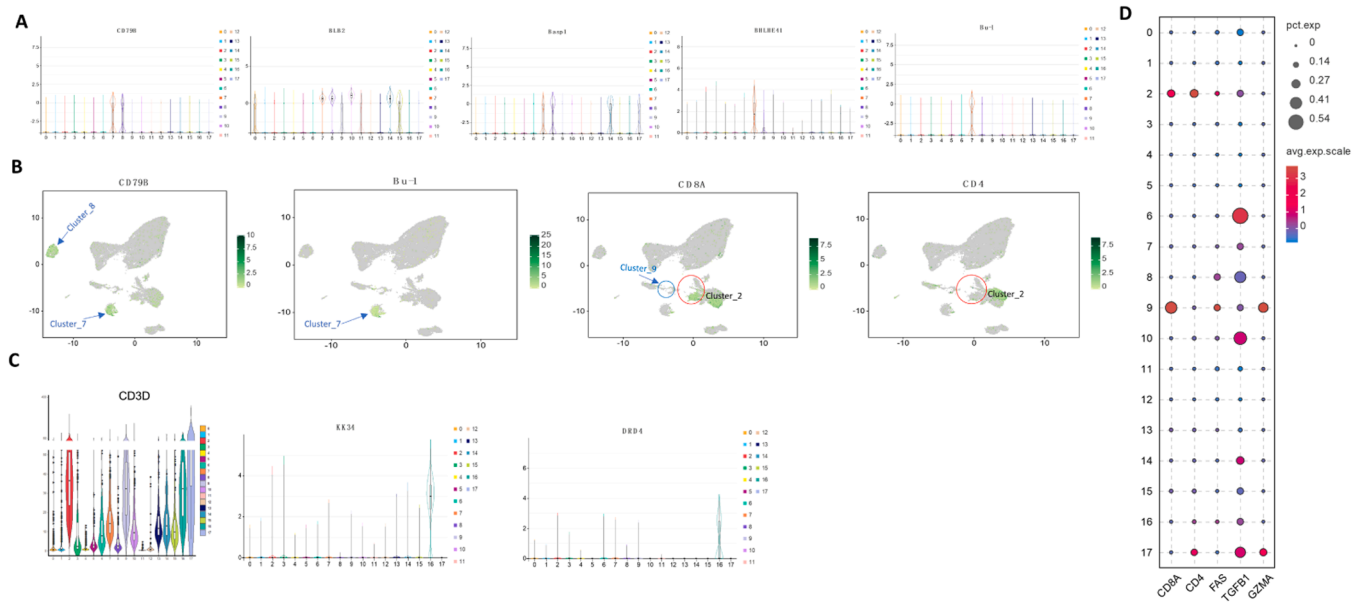

Fig. 2. ***Two B cell clusters and eight T cell clusters were identified.*** A: Violin plot showing the expression of characteristic marker genes (*CD79B, BLB2, Basp1, BHLHE41*, and *Bu-1*) in cluster. B: UMAP plot color-coded for expression (gray to green) of characteristic marker genes (*CD79B, Bu-1, CD8A*, and *CD4*). C: Violin plot showing the expression of characteristic marker genes (*CD3D, KK34*, and *DRD4*). D: Dot plot representing marker genes (*CD8A, CD4, FAS, TGFB1*, and *GZMA*) expressed in each cluster. Intensity represents the expression, and dot size represents the proportion of cells that expresses each gene.

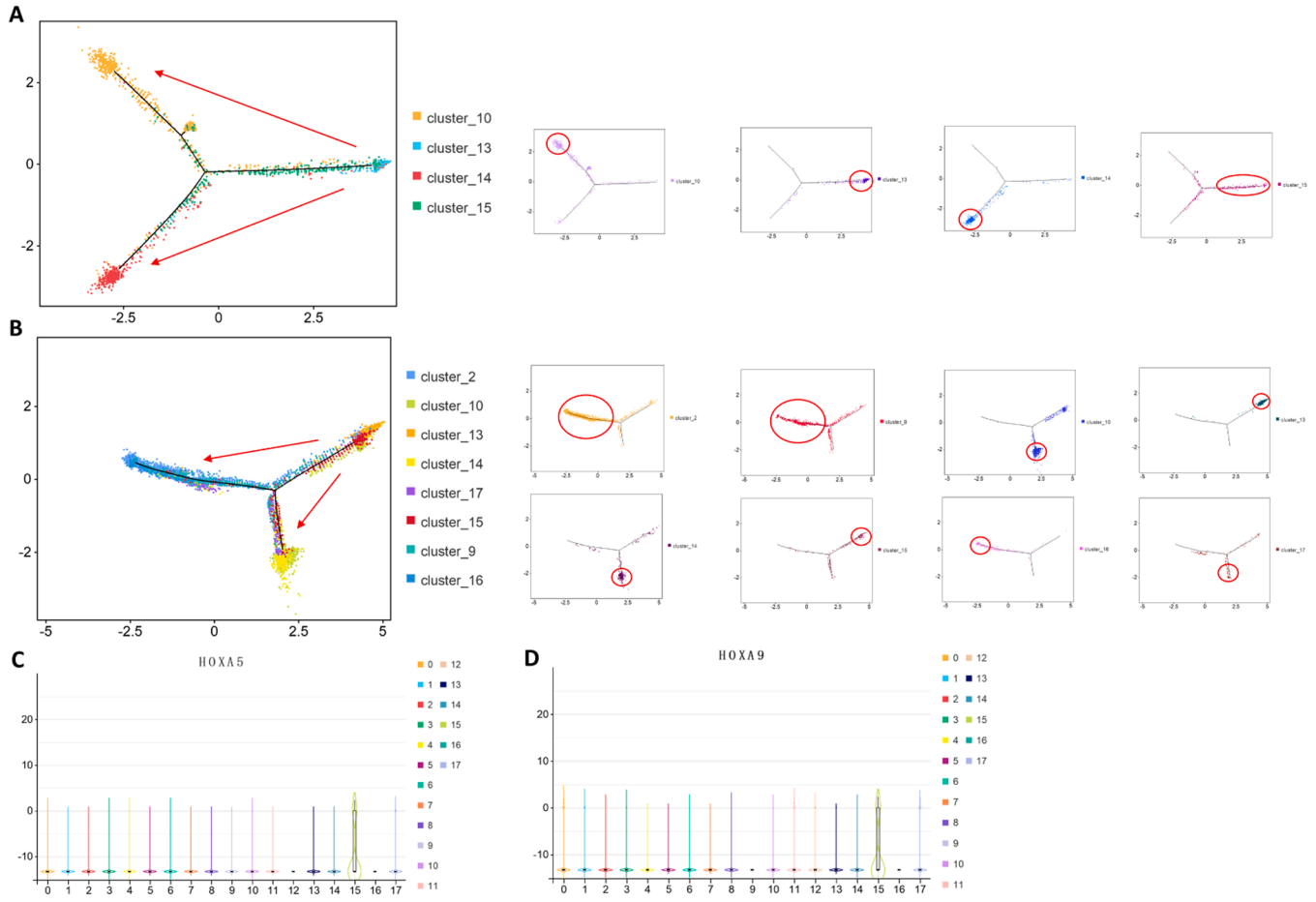

Fig. 3. ***Cluster_13 and cluster_15 identified as two progenitor-like T lymphocyte clusters.*** A: Mapping of four double-negative T cells (cluster_10, cluster_13, cluster_14, and cluster_15) to pseudotime trajectory. The red arrow in the Fig. represents the direction of differentiation. B: Mapping of eight T cells (cluster_2, cluster_9, cluster_10, cluster_13, cluster_14, cluster_15, cluster_16, and cluster_17) to pseudotime trajectory. C: Violin plot showing *HOXA5* expression in each cluster. D: Violin plot showing *HOXA9* expression in each cluster.

chicken regulatory T cells with low *CD25* expression but high *TGFB* expression (Gurung et al., 2017), similar to our findings (Figure S2). Therefore, Cluster_16 is hypothesized to be a Th2 cells with regulatory properties (also referred to as Treg-like Th2 cells). Cluster_17 had higher *CD4* and *TGFB1* expression than Cluster_16, and also expressed the cytotoxic protein gene *GZMA* (Fig. 2D), thus it was classified as a Cytotoxic CD4+ *T* cells with Treg-like features (also referred to as Treg-like cytotoxic CD4+ *T* cells). In Cluster_10, Cluster_13, Cluster_14, and Cluster_15, *CD3D* expression was high, but *CD4* and *CD8A* expression was low (Fig. 2C and D), so these cells were considered CD4−CD8− double-negative T cells. CD4−CD8− *T* cells are also referred to as double-negative T cells . Among these double-negative T cell clusters, Cluster_10 and Cluster_14 highly expressed *TGFB1* (Fig. 2D), and thus were classified as double-negative regulatory T cells.

Cluster_13 and cluster_15 identified as two progenitor-like T lymphocyte clusters

Considering the possibility of the presence of lymphocyte progenitor cells in the bone marrow, Monocle 2 was used to explore the potential differentiation relationships among multiple T cell clusters. First, pseudotime analysis was performed on four double-negative T cell clusters (cluster_10, cluster_13, cluster_14, and cluster_15). Cluster_13 and cluster_15 were concentrated together on one side of the cell trajectory, whereas cluster_14 and cluster_10 were concentrated separately on the other two sides (Fig. 3A). In the pseudotime analysis of the eight T cell subgroups, cluster_13 and cluster_15 were concentrated on the same side of the cell trajectory; cluster_10, cluster_14, and cluster_17 clustered together; and cluster_2, cluster_9, and cluster_16 clustered together (Fig. 3B). The classical genes *HOXA5* and *HOXA9* associated with hematopoietic stem/progenitor cell differentiation were highly expressed in cluster_15 (Fig. 3C and D). Despite the absence of classical genes associated with hematopoietic stem cell/progenitor cell differentiation detected on cluster_13, cluster_13 and cluster_15 were speculated to be progenitor-like T lymphocytes because they tended to be on the same side in the cell trajectory.

Cluster_0, cluster_1, cluster_3, cluster_11, and cluster_12 identified as tumor-like clusters

Considering the tumorigenic nature of ALV-J, tumor cells may be present in the samples. The top five genes of cluster_0, cluster_1, cluster_3, cluster_11, and cluster_12 were all associated with cancer (Table S3). Pearson's correlation analysis showed that cluster_0, cluster_1, cluster_3, cluster_11, and cluster_12 were highly correlated (Fig. 4A). In the subsequent cell cycle analysis, these five clusters exhibited high cell division capacity (Fig. 4B). The functional differences among the clusters were compared by GSVA to further determine whether these five clusters are tumor-like cells. The results showed that cluster_0, cluster_1, cluster_3, cluster_11, and cluster_12 had different pathway activities from other clusters. The pathways associated with cancer, such as "MYC_TARGETS", "G2M_CHECKPOINT", and "REACTIVE_OXIGEN_SPECIES_PATHWAY", were mainly concentrated in cluster_0, cluster_1, cluster_3, cluster_11, and cluster_12. In addition, compared with other subgroups, these five subgroups showed different metabolic reprogramming patterns, such as "FATTY_ACID_METABOLISM", "ADIPOGENESIS", and "OXIDATIVE_PHOSPHORYLATION" (Fig. 4C). In summary, cluster_0, cluster_1, cluster_3, cluster_11, and cluster_12 were hypothesized to be tumor-like clusters. Due to the lack of sufficient reference, cluster_4, cluster_5, and cluster_6 could not be defined. Among the five tumor-like clusters identified, Cluster_0 exhibited distinct molecular characteristics. The proto-oncogenes MYC and MYB were significantly upregulated in Cluster_0, while marker genes associated with abnormal cancer cell proliferation, such as KRAS, CDKN2A (P16), CCND1 (Cyclin D1), and CDK6, showed the most significant differential expression. Additionally, the expression level of the stemness gene SOX2 was markedly higher in Cluster_0 compared to other tumor subpopulations (Figure S3). These results suggest that Cluster_0 may represent a malignant cell population in the terminal stage of avian leukosis. Further analysis of the intercellular

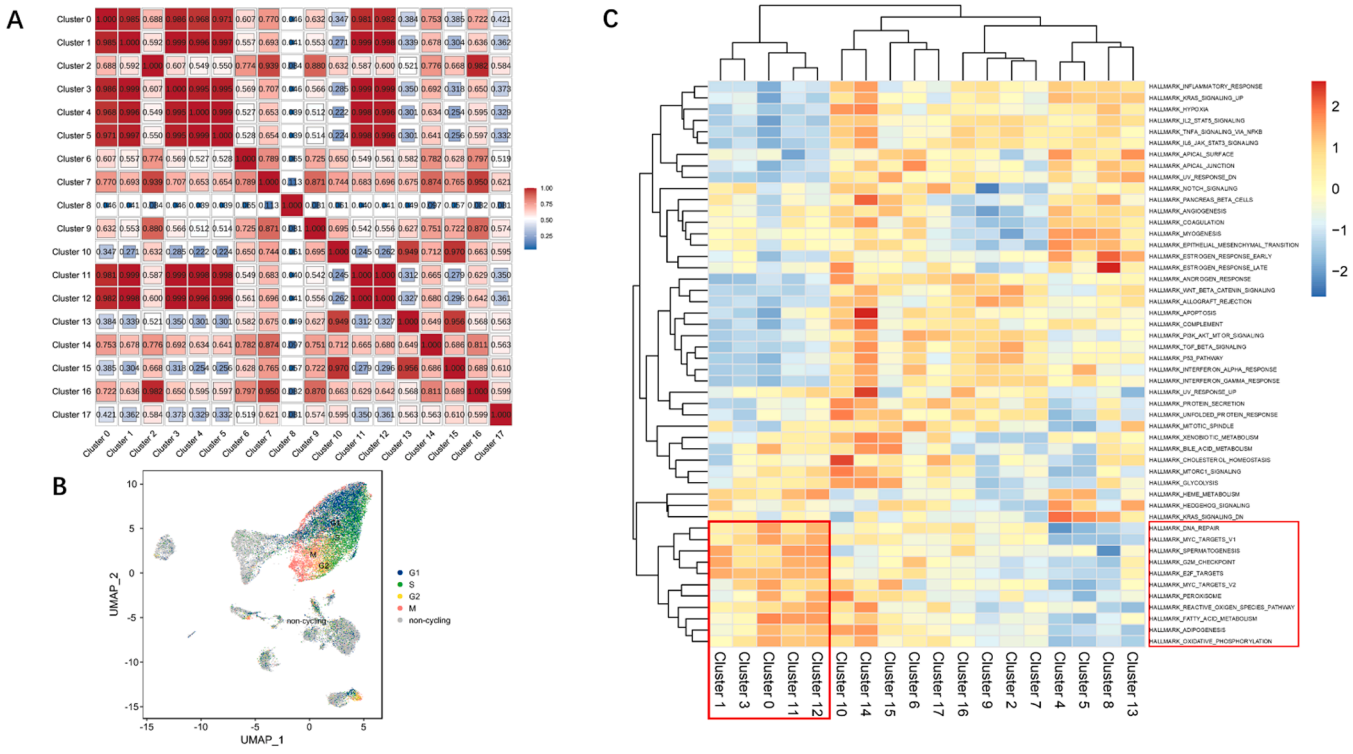

Fig. 4. ***Cluster_0, cluster_1, cluster_3, cluster_11, and cluster_12 identified as tumor-like clusters.*** A: Pearson's correlation analysis of different cell populations based on gene expression levels. B: UMAP plot showing the cell cycle status of each cell. C: Gene set variation analysis based on "HALLMARK".

communication network revealed that both the quantity and intensity of ligand-receptor interactions among cell subpopulations were significantly upregulated in the ALV group compared to the NC group (S4 A-D). Notably, CD99, an immunomodulatory molecule implicated in human myeloid and lymphoid leukemia, exhibited the strongest activity in cell communication signaling pathways within Cluster_0 (S4 E). Moreover, the CD99 was not only significantly upregulated in the ALV group but also showed significantly higher expression levels compared to the NC group(S4 F). This finding further supports the association of Cluster_0 with the malignant cell population in the terminal stage of avian leukosis and suggests that CD99 may play a critical role in the pathogenic mechanisms of ALV-J.

Lymphocyte clusters in bone marrow showing different responses to ALV-J infection

Among T lymphocytes, the T cell co-stimulatory molecules *CD28* and *ICOS* were highly expressed in cluster_2 and cluster_16 (Fig. 5A), and the T cell co-inhibitory molecule *CTLA4* was highly expressed in cluster_2 (Fig. 5B). The expression of cytokine genes was detected in lymphocytes. Cluster_2 expressed *IL16, XCL1, TGFB1*, and *IL18*; cluster_9 expressed *IL16, IL18*, and *XCL1*; cluster_10 and cluster_14 expressed *TGFB1, IL18*, and *IL15*; and cluster_7, cluster_16, and cluster_17 expressed *IL16* and *TGFB1* (Fig. 5A). Several subgroups expressed the immunosuppression-related molecules *IL16, TGFB1*, and *CTLA4* (Fig. 5A and B). The expression of *IL16, TGFB1*, and *CTLA4* was significantly higher in sample ALV than in sample NC (Table S4). Then, the expression of *IL16, TGFB1*, and *CTLA4* was examined by qRT-PCR, and the results showed that the expression of *IL16, TGFB1*, and *CTLA4* was higher in sample ALV's bone marrow (Fig. 5C). In the GO enrichment analysis for ten lymphocyte clusters with upregulated DEGs, nine lymphocyte clusters were highly enriched in the terms "immune system process" and "response to stimulus", except for cluster_13 (Fig. 5D). In the GO enrichment analysis of DEGs between samples ALV and NC, cluster_2, cluster_7, cluster_8, cluster_9, cluster_10, and cluster_15 were more enriched in "immune system process" and "response to stimulus" (Fig. 5E). In the KEGG enrichment analysis of upregulated DEGs in the 10 lymphocyte subgroups, cluster_2, cluster_7, cluster_8, cluster_9, cluster_16, and cluster_17 were enriched in the pathway associated with viral infection (Fig. 6A–F). Cluster_2, cluster_7, and cluster_9 not only accounted for a higher proportion of the two types of samples but also varied more between these two types (Fig. 1E). Subsequently, cluster_2, cluster_7, and cluster_9 were further analyzed.

Increased cluster_2 leading to immunosuppression environment in bone marrow microenvironment

The DEGs of cluster_2 between sample ALV and sample NC were calculated to explore the reason for the variation of cluster_2 between samples and the immune status between samples. A total of 716 significantly DEGs were identified, of which 393 were highly expressed in sample ALV (Fig. 7A). Among these DEGs, *CTLA4* and *FOS*, which promotes tumor-infiltrating T cell exhaustion (Xiao et al., 2012), had a higher expression in sample ALV (Fig. 7A). The GSEA enrichment analysis showed that cluster_2 was less immunoreactive in sample ALV. For instance, "complement activation", "classical pathway", and "phagocytosis, recognition" were more enriched in sample NC (Fig. 7B). However, cluster_2 had a high cell viability in sample ALV. For example, this sample was highly enriched in "cytosolic ribosome" and "ribosome" (Fig. 7B). In addition, the bone marrow homing receptor gene *CXCR4*; the T-cell-migration-related gene *GPR183*; and the genes promoting T cell production, namely, *TNFRSF9* and *IL18R*, were more highly expressed in sample ALV (Fig. 7A). In summary, cluster_2 was hypothesized to proliferate after migrating from peripheral tissues to the bone marrow, and that the increased cluster_2 led to an increased immunosuppressive state in the bone marrow microenvironment.

Visualization of *CD4* and *CD8A* clearly showed a portion of cells in cluster_2 expressing *CD4* and a portion of cells expressing *CD8A* (Fig. 2B). Then, subpopulation analysis of cluster_2 was performed. Cluster_2 was further divided into eight subpopulations, of which

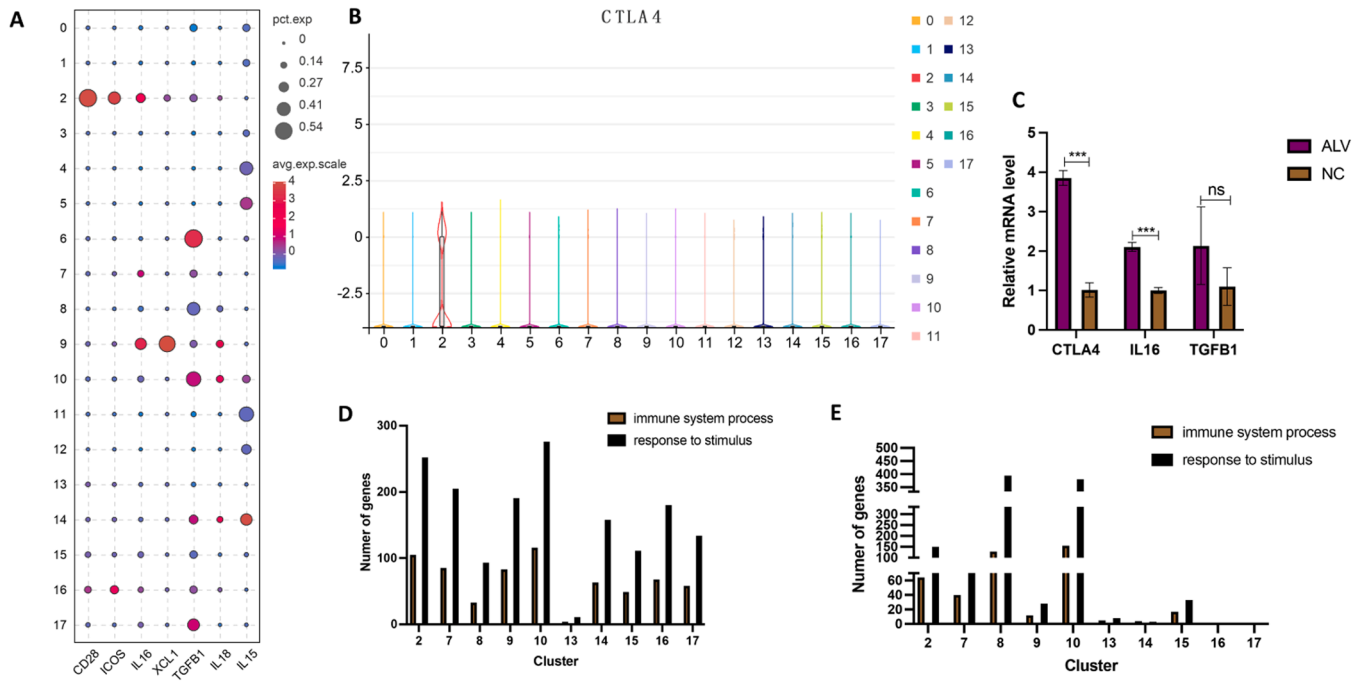

Fig. 5. ***Lymphocyte clusters in bone marrow showing different responses to ALV-J Infection.*** A: Dot plot representing selected genes (*CD28, ICOS, IL16, XCL1, TGFB1, IL18*, and *IL15*) expressed in each cluster. Intensity represents the expression, and dot size represents the proportion of cells expressing each gene. B: Violin plot showing *CTLA4* expression in each cluster. (C) *CTLA4, IL16*, and *TGFB1* expression, as examined by qRT-PCR. D: Statistics of upregulated DEGs involved in the GO terms "immune system process" and "response to stimulus", as analyzed in lymphocyte population. E: Statistics of DEGs (ALV vs. NC) involved in GO terms "immune system process" and "response to stimulus", as analyzed in lymphocyte population.

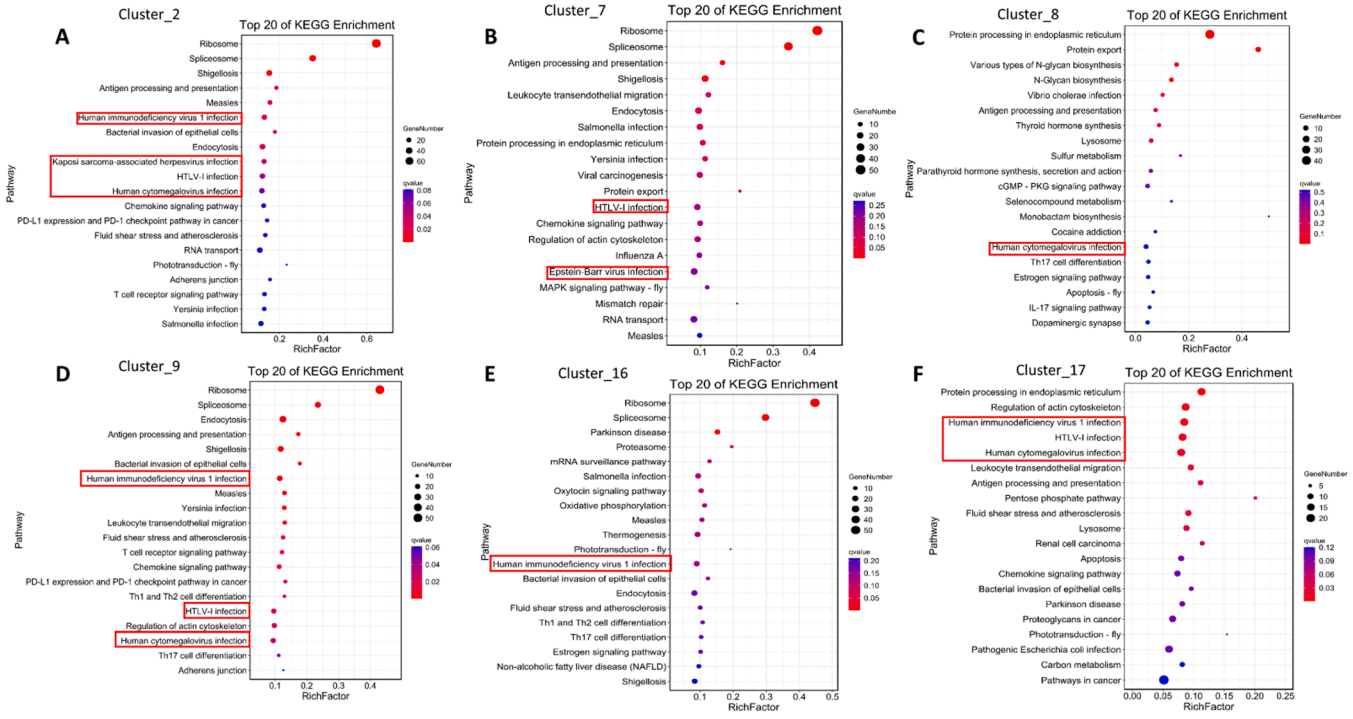

Fig. 6. ***Lymphocyte clusters in bone marrow showing different responses to ALV-J Infection.*** A–F: Top 20 significantly enriched KEGG pathways in cluster_2, cluster_7, cluster_8, cluster_9, cluster_16, and cluster_17.

cluster_2_0, cluster_2_1, cluster_2_2, and cluster_2_3 were higher in number, and each subpopulation was more abundant in sample ALV than in sample NC (Fig. 7C). In these eight subpopulations, cluster_2_0, cluster_2_3, cluster_2_6, and cluster_2_7 were found to be $CD4^{+}CD8^{+}T$ cells, cluster_2_1 was a $CD8^{+}$ *T* cell, cluster_2_2 was a $CD4^{+}T$ cell, and cluster_2_4 was a $CD4^{-}CD8^{-}T$ cell (Fig. 7D–F). Cluster_2_5 specifically highly expressed the Th2-related genes *KK34* and *DRD4* (Fig. 7G and H), suggesting that cluster_2_5 was a Th2-like cell. Then, these eight subpopulations were characterized with their top five upregulated DEGs (Fig. 7I). Within these eight subpopulations, *CD28* and *CTLA4* were highly expressed in cluster_2_0, cluster_2_2, cluster_2_3, cluster_2_4, cluster_2_6, and cluster_2_7. *ICOS* was highly expressed in cluster_2_0, cluster_2_2, cluster_2_3, cluster_2_6, and cluster_2_7 (Fig. 7J–L). These eight subpopulations exhibited different cytokine gene expression profiles. Cluster_2_1 and cluster_2_2 expressed higher levels of cytokine genes. Cluster_2_1 mainly expressed *IL16, IL18, XCL1*, and *CCL4*, although it also expressed *TGFB1* to some extent; *TGFB1* was relatively high in cluster_2_3 and cluster_2_4; and cluster_2_2 expressed higher levels of cytokine genes *IL16* and *IL18* (Fig. 7M).

Cluster_9 playing a role in resistance to ALV-J infection

The DEGs of cluster_9 between sample ALV and sample NC were calculated. A total of 91 significantly DEGs were identified, of which 68 were highly expressed in sample ALV (Fig. 8A). $CD8^{+}T$-cell-proliferation-related genes *B2M* (Theodoratos et al., 2010) and *CCL4* (Castellino et al., 2006) were significantly upregulated in sample ALV (Fig. 8A). Classical cytotoxicity-related genes CD44, GZMK, and CD8A were more highly expressed in sample ALV (Fig. 8A). GSEA also showed that the splitting activity of sample ALV was stronger than that of sample NC. For example, "cell cycle" was enriched in sample ALV (Fig. 8B). "Oxidative phosphorylation", "protein processing in endoplasmic reticulum", and other cytotoxicity-related terms were enriched to a higher extent in sample ALV (Fig. 8C). Ribosome-related GSEA terms, such as "structural constituent of ribosome" and "cytosolic ribosome", were also enriched to a higher extent in sample ALV (Fig. 8C). In the GO enrichment analysis, the DEGs were mostly concentrated in terms of electron respiratory chain and mitochondrial membrane (Fig. 8D). The PPI of DEGs revealed that *PRDX1*, a gene associated with $CD8^{+}T$ cell resistance to infection, was at the core of the network (Fig. 8E), and this gene was upregulated in sample ALV (Fig. 8A). In addition, the transcription- and translation-related hub genes *EEF1B2, RPLP0, EEF1A1*, and *GNB2L1* in the PPI network were upregulated in sample ALV (Fig. 8A and D). In summary, when an infection of ALV-J occurs, the number of cytotoxic T cells in the bone marrow increases and the cytotoxicity is more intense.

Cluster_7 showing resistance to ALV-J infection

The DEGs of cluster_7 between sample ALV and sample NC were determined, and a total of 256 DEGs were found (229 were upregulated in sample ALV, Fig. 9A). IPA analysis of the DEGs revealed that the pathways associated with cell migration and cellular activity, such as "cell movement", "cell movement of lymphocytes", and "EIF2 signaling", were increased in sample ALV (Fig. 9B and C). Moreover, chicken B- cell-migration- and maturation-related genes *CXCR4* (Laparidou et al., 2020) and *KLF2* (Wittner and Schuh, 2021) were significantly upregulated in sample ALV (Fig. 9A). GSEA also showed that sample ALV had higher activity and proliferation capacity than sample NC, such as "ribosome", "structural constituent of ribosome", "cytosolic ribosome", "DNA methylation", and "oxidative phosphorylation" (Fig. 9D). Moreover, "antigen processing and presentation", "antimicrobial humoral response", and "viral protein interaction with cytokine and cytokine receptor" were more enriched in sample ALV (Fig. 9D).

CD3D had a low expression in cluster_7 (Fig. 2C). Subsequently, a subpopulation analysis of cluster_7 was conducted. Cluster_7 was further divided into three subgroups, namely, cluster_7_0, cluster_7_1, and cluster_7_2, with cluster_7_0 accounting for the vast majority (Fig. 9E). Among the upregulated DEGs, the top five DEGs for cluster_7_1 was associated with T cells (Fig. 9F). Cluster_7_1 specifically expressed *CD3E, CD4, CD8A*, and *UBASH3A* (the gene encoding the T-cell ubiquitin ligand protein family, Fig. 9G). Cluster_7_1 also highly expressed B-cell-

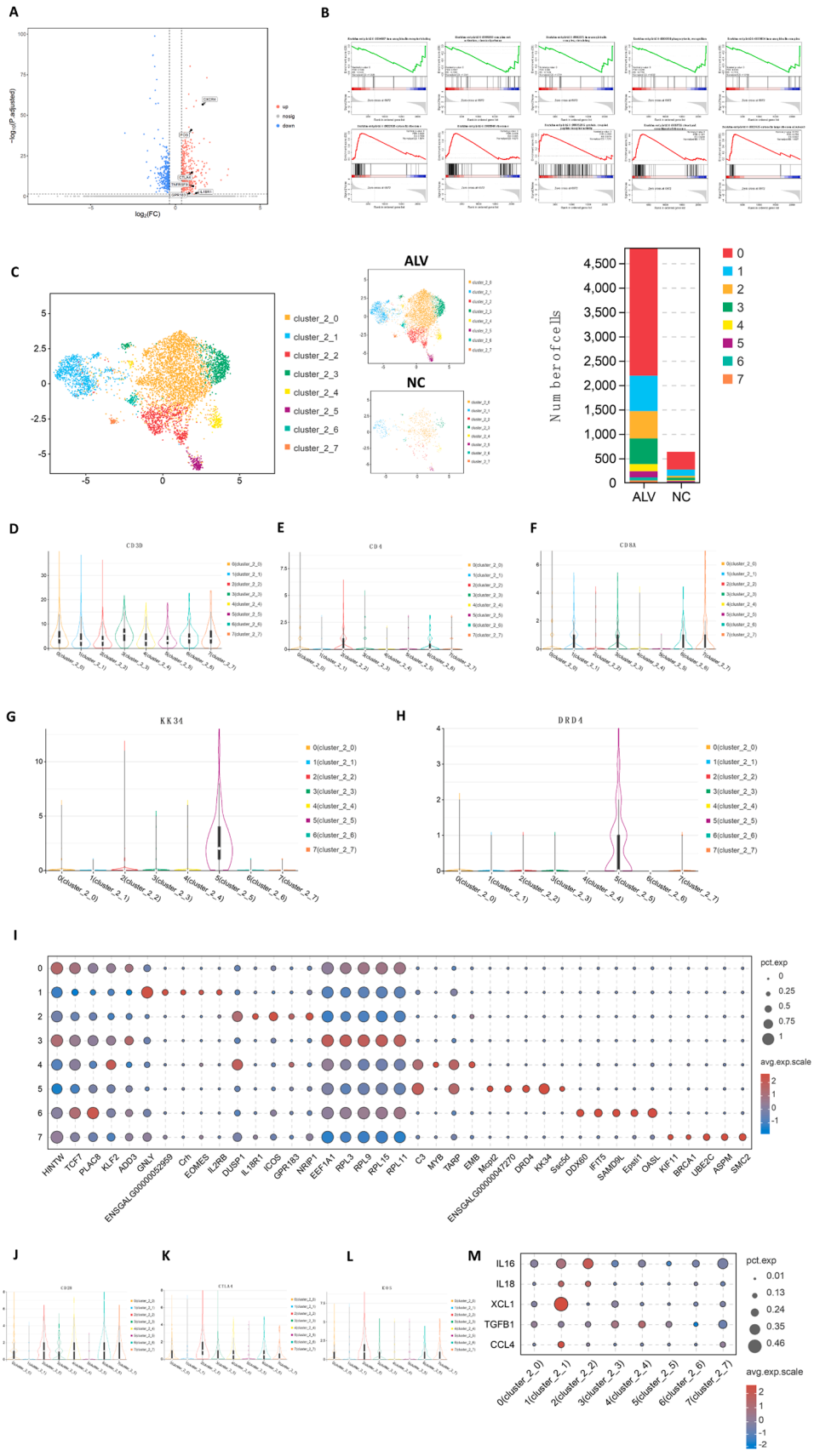

(caption on next page)

Fig. 7. ***Increased Cluster_2 leading to immunosuppression environment in bone marrow microenvironment.*** A: Volcano plots indicating significant DEGs in cluster_2 of different sample. B: GSEA of cluster_2 in samples ALV and NC. Negative enrichment for genes related with immune, positive enrichment for genes related with cell viability. C: UMAP display of cluster_2 subpopulation and its proportion in samples ALV and NC. D–H: Violin plot showing the expression of characteristic marker genes (*CD3D, CD4, CD8A, KK34*, and *DRD4*) in cluster_2 subpopulation. I: Top five DEGs identified in cluster_2 subpopulation. Dot size represents the proportion of cells in the cluster that expresses the gene; intensity indicates the mean expression. J–L: Violin plot showing the expression of *CD28, CTLA4*, and *ICOS*. (M) Dot plot representing cytokine expression in each subpopulation.

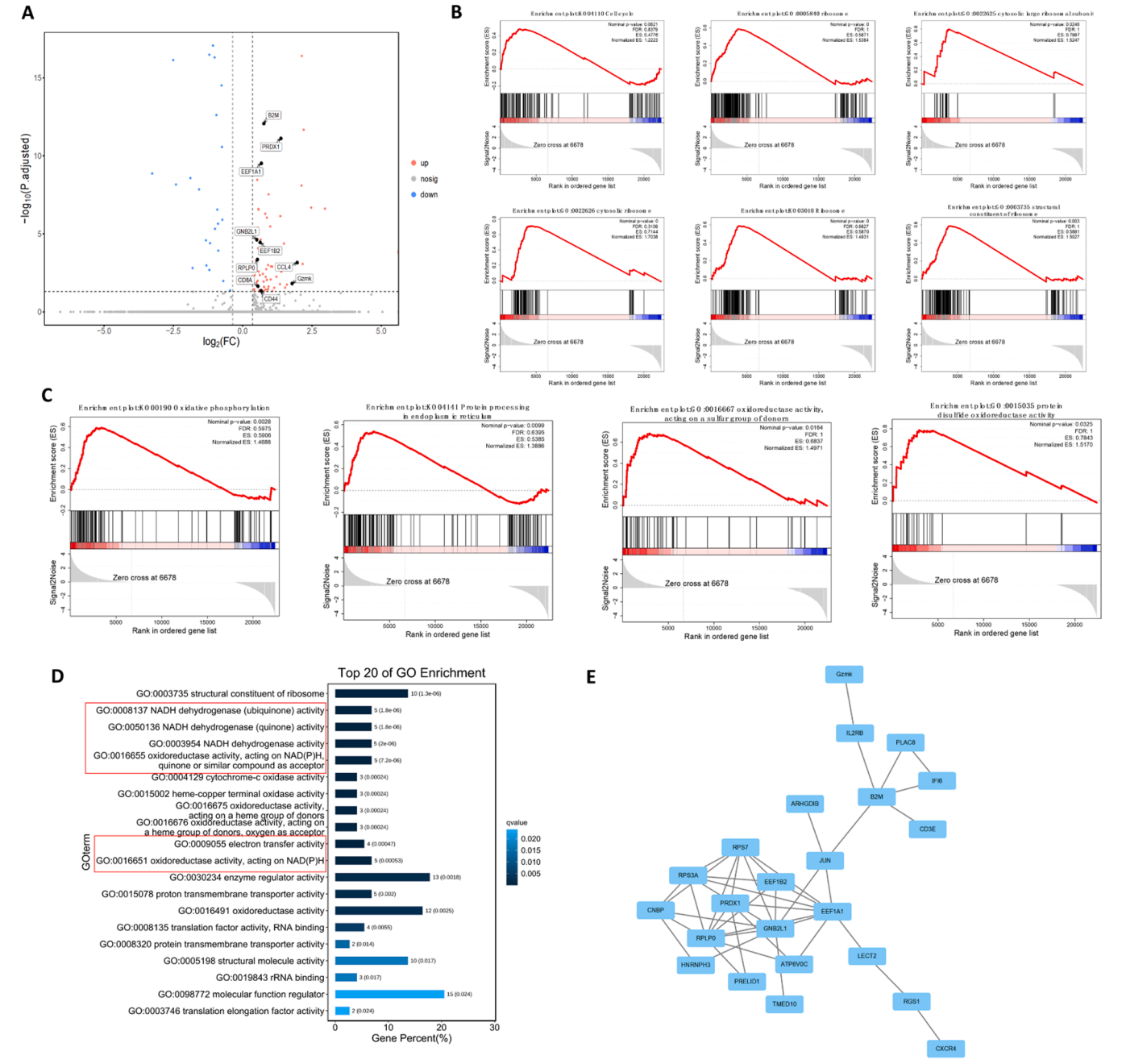

Fig. 8. ***Cluster_9 playing a role in resistance to ALV-J infection.*** A: Volcano plots indicating significant DEGs in cluster_9 of different sample. B: GSEA of cluster_9 in samples ALV and NC. Positive enrichment for genes related with cell division activity. C: GSEA of cluster_9 in samples ALV and NC. Positive enrichment for genes related with ribosome and cell viability. D: GO enrichment analysis of DEGs in cluster_9 of different samples. E: PPI network showing interactions between proteins based on gene expression.

related genes, such as *CD79B, Bu-1, BHLH41*, and *BCL11A* (Fig. 9H). Subsequently, *CD4* and *Bu-1* co-expressing cells were identified by immunohistochemistry (Fig. 9I).

The IPA analysis of upregulated DEGs across cluster_7_1 showed that in the top 10 "canonical pathways", the pathways related to cell proliferation, cell function, and cell development were activated, such as "IL-7 signaling pathway" and "signaling by Rho family GTPases". In addition, the pathways related to Th1 and Th2 were activated (Fig. 10A). In the "disease and function" module, the DEGs were mostly related to cell proliferation, such as "proliferation of lymphocytes",

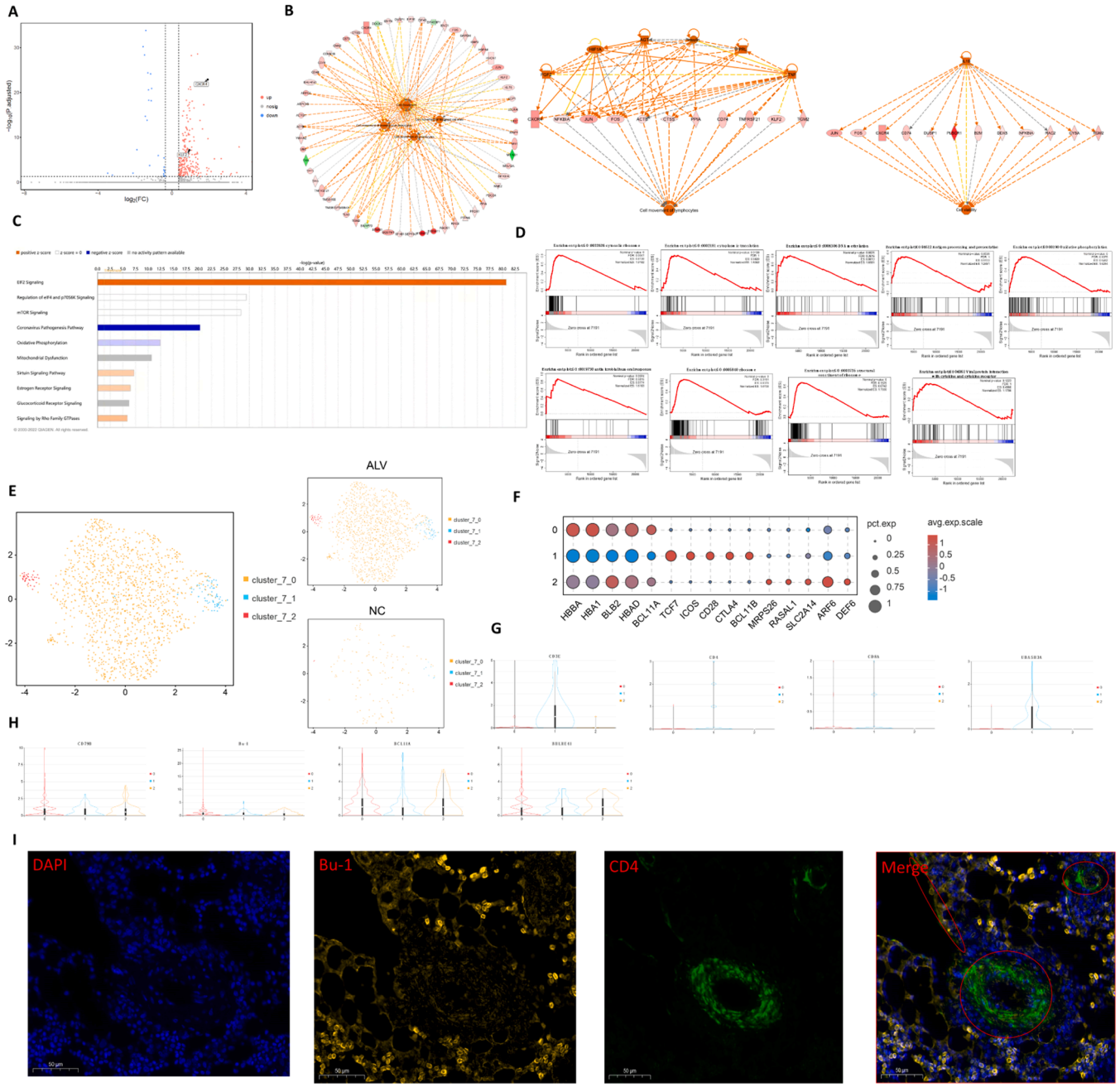

Fig. 9. ***Cluster_7 showing resistance to ALV-J infection.*** A: Volcano plots indicating significant DEGs in cluster_7 of different samples. B: Predicted network showing numerous genes related with cell migration. C: Top 10 canonical pathway predicted by IPA. Orange indicates activation, and blue indicates inhibition (the darker the color, the deeper the activation or inhibition). D: GSEA of cluster_9 in samples ALV and NC. E: UMAP display of cluster_7 subpopulation in samples ALV and NC. F: Top five DEGs identified in cluster_7 subpopulation. Dot size represents the proportion of cells in the cluster that expresses the gene; intensity indicates the mean expression. G and H: Violin plot showing the expression of characteristic marker genes (*CD3E, CD4, CD8A, UBASH3A, CD79B, Bu-1, BCL11A*, and *BHLHE41*) in cluster_7 subpopulation. I: Immunohistochemical staining, yellow-Bu-1, green-CD4.

"proliferation of immune cells", and "quantity of lymphocytes" (Fig. 10B). By using IPA, several upstream regulators associated with cell proliferation were predicted, such as *EGF, AHR*, and *CCND1* (Fig. 10C). Thus, cluster_7_1 expressed B cell marker genes and T cell marker genes, probably as a result of abnormal cell proliferation.

Different clusters and cells of the same cluster showing different susceptibilities to ALV-J

The infection rate of each subgroup to the virus was assessed by calculating the UMI of ALV-J. The viral infection rate of cluster_6, cluster_9, cluster_10, and cluster_16 exceeded 50 %, with cluster_6 having the highest percentage of cells with high viral load (Fig. 11A). In addition, in the same subgroup, the viral infection rate was higher in sample ALV (Fig. 11B). The cells in the same cluster exhibited different infection rates, with some cells showing no viral load and some having high viral load (Fig. 11A). For investigation as to why part of cells in the same cluster expressed viral transcripts whereas others did not, the DEGs for each cluster in cells with and without viral load were calculated. The results showed that the DEGs differed greatly within clusters (Table S5). However, co-expressed DEGs were not found in each cluster.

Next, IPA analysis was performed on 12 subgroups (cluster_0,

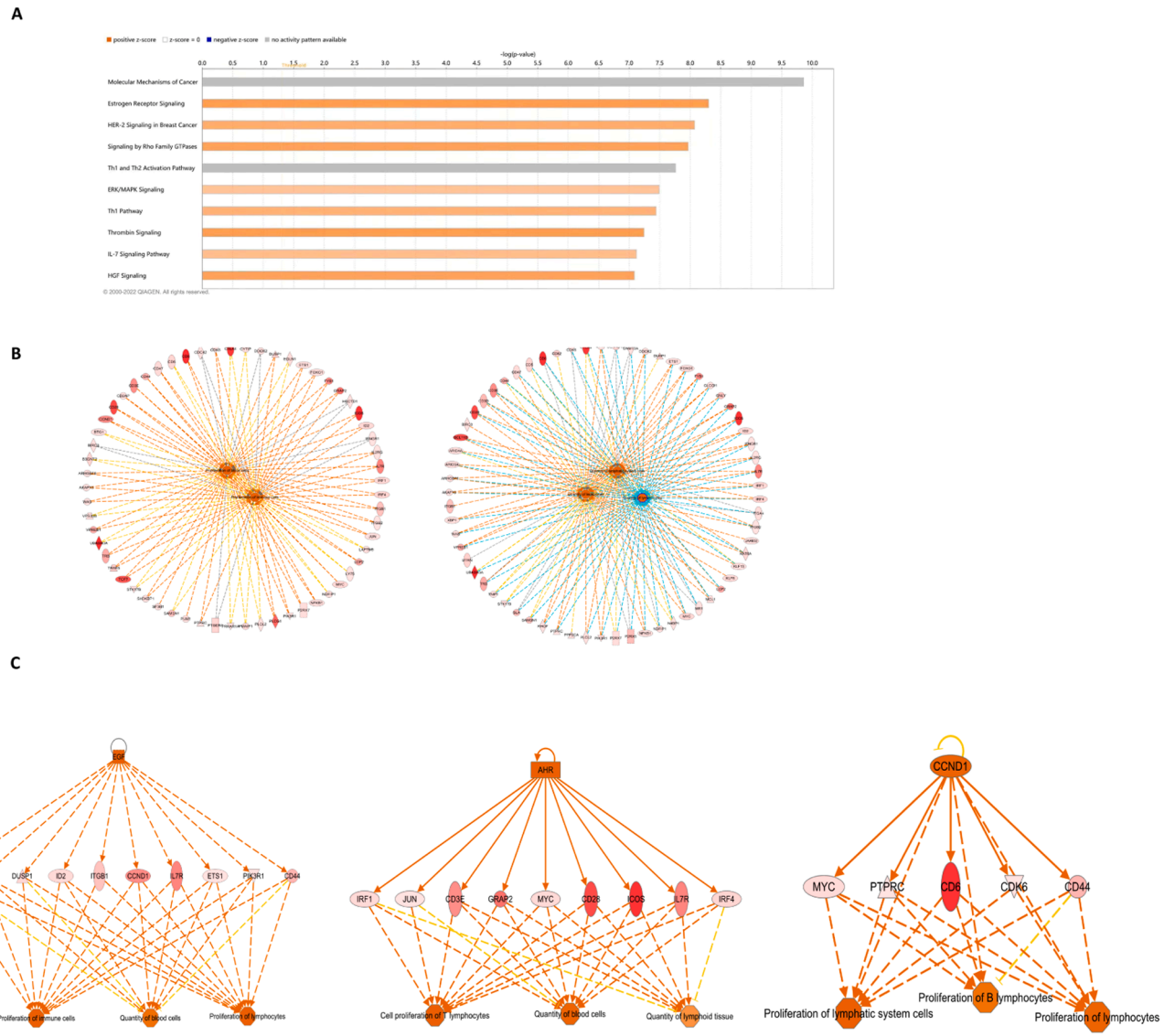

Fig. 10. ***Cluster_7 showing resistance to ALV-J infection.*** A: Top 10 canonical pathway predicted by IPA. Orange indicates activation. B: Predicted network showing numerous genes related with cell proliferation. C: Predicted upstream regulatory factors by IPA (*EGF, AHR*, and *CCND*).

cluster_1, cluster_3, cluster_4, cluster_5, cluster_6, cluster_8, cluster_10, cluster_11, cluster_12, cluster_14, and cluster_15) with a high number of DEGs. The top 10 canonical pathways were active in the vast majority of the analyzed subgroups, such as "signaling by Rho family GTPases" and "estrogen receptor signaling" (Fig. 11C). The predicted downstream "diseases and functions" associated with cell death were inhibited, such as "organismal death", "apoptosis" and "necrosis". More importantly, "diseases and functions" associated with viral infections were activated, such as "viral infection", "infection by RNA virus", and "infection by HIV-1" (Fig. 11D). Among the predicted upstream regulators, the proto-oncogenes *MYC* and *MYCN* were activated globally; *RICTOR* and *LARP1* were repressed globally; and the lymphocyte-related upstream regulators *CD40, CD3*, and *BCR* were activated globally (Fig. 11E). The above results suggested a possibly large heterogeneity in the susceptibility of cells in chickens to ALV-J, but the reasons for this need to be further explored.

Discussion

In recent years, scholars generally agree that abnormal changes in immune cells within the bone marrow microenvironment are closely associated with the development of leukemia (Hawkins et al., 2016; Hohtari et al., 2019; Lamble et al., 2020). ALV can induce various tumorigenic diseases, including leukemia. Therefore, to investigate the mechanisms by which ALV infection affects immune cells within the bone marrow microenvironment, this study used 10x single-cell RNA sequencing to analyze the composition of chicken bone marrow lymphocytes under ALV-J infection and explore the immune responses of these lymphocytes, as well as the immune mechanisms triggered by viral infection.

By analyzing the single-cell RNA sequencing data, this study identified 18 cell clusters isolated from chicken lymphocytes. As the isolation of chicken lymphocytes was based on density gradient centrifugation, not all of the 18 clusters were lymphocytes. Two B cell clusters (Cluster_7: B1-like cells; Cluster_8: plasma cell-like cells), eight T cell clusters (Cluster_2: double-positive T cells; Cluster_9: cytotoxic T cells; Cluster_10: double-negative regulatory T cells; Cluster_13: progenitor-like T cells; Cluster_14: double-negative regulatory T cells; Cluster_15: progenitor-like T cells; Cluster_16: Treg-like Th2 cells; Cluster_17: Treg-like cytotoxic CD4+ *T* cells), and five tumor-like cell clusters (Cluster_0, Cluster_1, Cluster_3, Cluster_11, and Cluster_12) were defined. Additionally, three undefined clusters were observed (Cluster_4, Cluster_5,

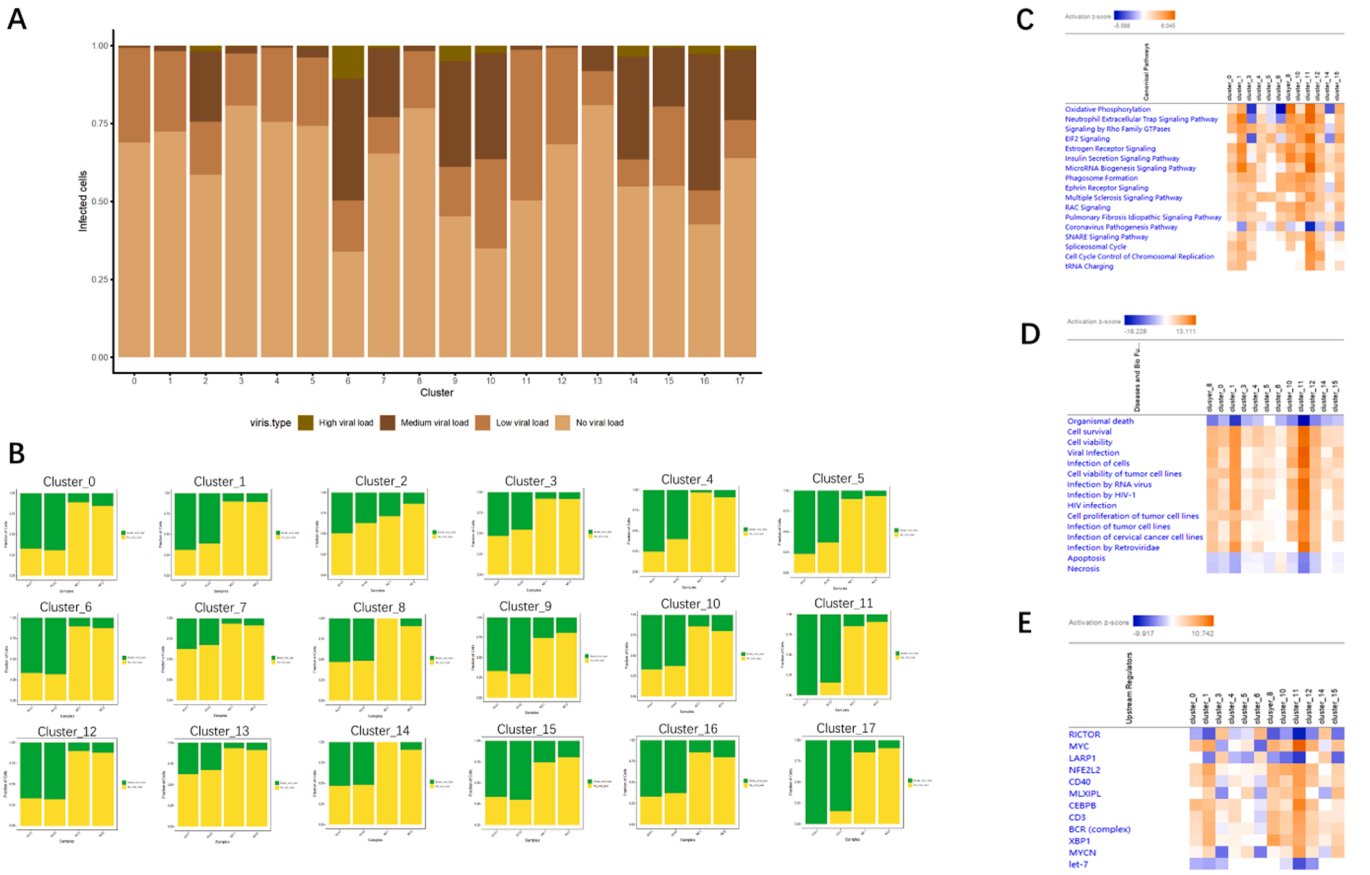

Fig. 11. ***Different clusters and cells of the same cluster showing different susceptibilities to ALV-J.*** A: Heat map showing the viral load in each cluster. The darker the color, the higher the viral load. B: Fraction of cells with and without viral load of each cluster in each sample. Green represents "viral load exists", and yellow represents "no viral load". C: Comparison analyses of 12 clusters in "canonical pathway". From left to right: cluster_0, cluster_1, cluster_3, cluster_4, cluster_5, cluster_6, cluster_8, cluster_10, cluster_11, cluster_12, cluster_14, and cluster_15. D: Comparison analyses of 12 clusters in "diseases and biological pathways". From left to right: cluster_0, cluster_1, cluster_3, cluster_4, cluster_5, cluster_6, cluster_8, cluster_10, cluster_11, cluster_12, cluster_14, and cluster_15. E: Comparison analyses of 12 clusters in "predicted upstream regulators". From left to right: cluster_0, cluster_1, cluster_3, cluster_4, cluster_5, cluster_6, cluster_8, cluster_10, cluster_11, cluster_12, cluster_14, and cluster_15.

and Cluster_6; Fig. 1A–C).

The identification of four regulatory T cell subpopulations (Cluster_10, Cluster_14, Cluster_16, and Cluster_17) was based on the expression of *TGFB1*, though studies on chicken regulatory T cells are limited, and the understanding is not yet comprehensive. Some studies have suggested that chickens do not express the regulatory T cell marker gene *FOXP3* (Lopes et al., 2006), though recent studies have detected *FOXP3* expression in chickens (Burkhardt et al., 2022). Previous studies have commonly identified chicken regulatory T cells by *CD25*, but during immune responses to MDV infection, a subgroup of regulatory T cells expressing high levels of TGFB but low *CD25* expression was identified (Gurung et al., 2017), This finding is consistent with the results of the present study (Figure S2). Thus, in this study, T cells expressing high levels of *TGFB* were uniformly considered as regulatory T cells. In the future, we can further investigate the functional characteristics of these Tregs subpopulations and their mechanisms in immune regulation under conditions of varying viral infection severity using single-cell multi-omics technologies.

Since there are no reports of chicken lymphocyte progenitors, the identification of lymphocyte progenitors (Cluster_13 and Cluster_15) in this study was primarily based on pseudotime analysis results and mammalian lymphocyte stem cell marker genes. In the pseudotime analysis of four double-negative T cells and eight T cell clusters, Cluster_13 and Cluster_15 clustered at one end of the pseudotime axis, with Cluster_15 expressing the classical genes *HOXA5* and *HOXA9* associated with hematopoietic stem cell differentiation (Fig. 3). Therefore, Cluster_13 and Cluster_15 were identified as progenitor-like cells. However, it is noteworthy that *HOXA5* and *HOXA9* are not only classical genes for hematopoietic stem cells but are also associated with tumors (Ko et al., 2012; Moorthy et al., 2023; Pai et al., 2022; Ye et al., 2023). Further experiments are required to verify these findings. A specific subpopulation expressing both T cell and B cell marker genes was identified in ALV samples (Fig. 9G–I). The analysis suggested that this subpopulation may result from abnormal cell proliferation (Fig. 10). Similar subpopulations have been identified in breast cancer, where they are also in an abnormal proliferative state (Bassez et al., 2021).

In the identification of tumor cells, we determined that Cluster_0 represents a malignant cell population in the terminal stage of avian leukemia based on transcriptomic signature analysis of tumor-specific molecular markers (Figure S3). Further cell-cell communication analysis revealed that the CD99 signaling pathway exhibits significant levels of cellular communication within Cluster_0 (Figure S4 E). Substantial evidence supports the critical role of human CD99 in bone marrow and lymphocytic leukemia (Ali et al., 2022). This finding not only provides stronger evidence that Cluster_0 represents the malignant cell population in the terminal stage of avian leukemia but also suggests a potential association between CD99 and the pathogenic mechanisms of ALV-J.

In the resistance of chickens to MDV infection, key immune cells include macrophages (which inhibit viral replication by producing NO) and CD8+ *T* cells (which directly clear infected cells) (Schat and Xing, 2000). In HIV patients, a class of broadly specific cytotoxic T cells (**HXTCs**) plays an important role in clearing HIV-infected cells, with

HXTCs predominantly composed of CD8+ *T* cells (89.1 %) and a smaller proportion of CD4+ *T* cells (7.4 %) (Sung et al., 2015). In this study, among the ten lymphocyte subpopulations, only Cluster_2, Cluster_7, Cluster_8, Cluster_9, Cluster_10, and Cluster_15 were enriched in the terms "immune system process" and "response to stimulus," and only Cluster_2, Cluster_7, Cluster_9, Cluster_16, and Cluster_17 were enriched in pathways related to viral infections. Of these, Cluster_2, Cluster_7, and Cluster_9 had higher proportions and greater variation between samples (Figs. 1E, 5 D, and 6). Therefore, double-positive T cells, B1-like B cells, and regulatory T cells may be key subpopulations involved in ALV-J infection.

Based on the study results, double-positive T cells, B1-like B cells, and regulatory T cells are proposed as key lymphocytes contributing to the immunosuppressive state in the bone marrow microenvironment. These three cell types express the immunosuppressive factor *TGFB1* (Fig. 2D), and research shows that the main function of the *TGFB* family is to inhibit the proliferation of T and B cells and suppress the function of macrophages, dendritic cells, and natural killer cells (Yoshimura and Muto, 2011). *TGFB1* has been shown to inhibit T cell proliferation, activation, and differentiation (Li et al., 2007). In addition to expressing *TGFB1*, Cluster_2 (double-positive T cells) and Cluster_7 (B1-like B cells) also express *IL16* (Fig. 5A), which preferentially induces the migration of TGFB-secreting regulatory T cells and can directly suppress T cell activity to some extent (Matsumoto et al., 2009; McFadden et al., 2007; Richmond et al., 2014). Cluster_2 also expresses the immunosuppressive molecule *CTLA4* (Fig. 5B). This molecule shares the same ligands (CD80/CD86) as the immune co-stimulatory molecule CD28, but *CTLA4* binds CD80/CD86 with a stronger affinity, thereby inducing T cell exhaustion (Liu and Xu, 2020; Merwe and Davis, 2003; Teft et al., 2006; Yokosuka et al., 2010). In hematological cancers, the immunosuppressive bone marrow microenvironment promotes the proliferation and survival of multiple myeloma (**MM**) and acute myeloid leukemia (**AML**) cells (Isidori et al., 2014; Tai et al., 2016). Studies suggest that the more severe the immunosuppressive state of the bone marrow microenvironment, the worse the clinical symptoms in AML patients (Isidori et al., 2014). In this study, clinical symptoms in ALV samples also worsened as the immunosuppressive state intensified. Although Cluster_7 expresses immunosuppressive cytokines, it also shows resistance to ALV-J infection. GSEA enrichment analysis revealed that, in Cluster_7, pathways associated with antiviral infection were more enriched in the ALV samples (Fig. 9D). This paradox is also observed in tumor-associated M2 macrophages, which release various immunosuppressive factors in tumor tissues but also demonstrate some disease resistance, though overall exacerbating tumor progression (Chung et al., 2023). However, whether Cluster_7 exacerbates or alleviates ALV-J infection needs to be verified in subsequent experiments.

The study also found that four regulatory T cell subpopulations showed increased proportions in ALV samples. Regulatory T cells (**Tregs**) are a type of lymphocyte that induces immunosuppression. In the bone marrow microenvironment of MM or AML patients, Tregs contribute to cancer-related immune dysfunction (Braga et al., 2012; Corradi et al., 2022). Promoting Treg depletion in the bone marrow microenvironment can prevent MM cell dissemination (Dahlhoff et al., 2022). In a mouse model of AML leukemia, blocking Treg migration to the bone marrow microenvironment with drugs can delay AML progression (Wang et al., 2020).

The study found that Cluster_9 (cytotoxic T cells) plays an important role in resisting ALV-J infection. It highly expresses cytotoxicity-related genes *GNLY* and *GZMA*. *GNLY* is a granulysin protein synthesized by cytotoxic T cells, which lyses infected cells by affecting the activity of ion channels in the cell membrane (Krensky and Clayberger, 2009). In mouse studies, *GZMA* was found to induce infected cell death through perforin-mediated apoptosis (Pardo et al., 2002; Voskoboinik et al., 2015). Although Cluster_9 was found to increase in ALV samples, the clinical symptoms in these samples were more severe, possibly because the strong immunosuppressive effect of the bone marrow microenvironment outweighed the positive effects of cytotoxic T cells.

The immunosuppressive bone marrow microenvironment provides shelter for cancer cell proliferation, metastasis, and viral immune evasion. In this study, the bone marrow microenvironment in ALV samples was in a more immunosuppressed state, and two chickens in the ALV samples exhibited more severe clinical symptoms. Similarly, in patients with acute myeloid leukemia, the higher the proportion of T cells expressing immunosuppressive molecules *CTLA4* and *PD1* in the bone marrow microenvironment, the lower the survival rate of patients (Lamble et al., 2020). Although there are currently no reports of immune cells in the bone marrow microenvironment reacting with the virus, T cell exhaustion in the tumor microenvironment of HBV-induced hepatocellular carcinoma can lead to HBV evasion from the immune system (Kuipery et al., 2020).

This study also found that different subpopulations exhibited varying susceptibilities to ALV-J. Cluster_6, Cluster_9, Cluster_10, and Cluster_16 are the four subpopulations susceptible to ALV-J, all showing viral infection rates exceeding 50 % (Fig. 11A). In HIV infection, HIV exhibits unique susceptibility to CD4+ *T* cells, as *CD4* is the receptor for HIV (Bassez et al., 2021). However, in this study, the receptor gene for ALV-J, chNHE1, did not show differential expression between subpopulations. Further studies on HIV revealed that HIV entry into cells depends not only on its receptor *CD4* but also on co-receptors *CCR5* and *CXCR4* to assist entry (Grivel et al., 2000; Okoye and Picker, 2013). In this study, it was speculated that ALV-J may also employ a similar co-receptor mechanism, where even cells within the same subpopulation show different susceptibilities to ALV-J. IPA analysis of this phenomenon showed that "Rho family GTPase signaling pathway" was activated in all analyzed subpopulations (Fig. 11C). Rho GTPases control multiple signal pathways involved in gene expression, cell migration, cell proliferation, and cell survival and their role is related to nearly all stages of cancer development and progression (Haga and Ridley, 2016; Hodge and Ridley, 2016; Jansen et al., 2018; Pan et al., 2004; Rathinam et al., 2011; Vega and Ridley, 2008). The upregulation of several Rho GTPase family members with oncogenic activity and the downregulation of others with tumor-suppressive functions are frequently observed in cancer (Del Pulgar et al., 2005). Additionally, multiple studies have shown that GTPases play a crucial role in resisting viral infections. The Rab GTPase protein family is a major regulator of intracellular membrane dynamics (Bearer and Wu, 2019), and intracellular viral transport depends on the role of intracellular membranes, which HSV uses to enter the nucleus for replication and transcription (Cheng et al., 2011). Rab GTPases can also regulate the entry of Ebola virus and vesicular stomatitis virus into cells (Quinn et al., 2009). An article suggested that studies on how cells mitigate viral infections could start with the Rab GTPase protein family (Bearer and Wu, 2019). Although no studies have linked the Rab GTPase protein family to anti-ALV infection, the DEGs in this study were significantly enriched in pathways related to viral infection. The Rab GTPase protein family may play a crucial role in anti-ALV infection, although this hypothesis requires further validation in subsequent experiments.

In conclusion, this study performed an in-depth data analysis of chicken bone marrow lymphocytes under ALV-J infection using single-cell RNA sequencing, and through this data analysis, the composition of bone marrow cell subpopulations, ALV-J virus-responsive cell populations, and molecular immune mechanisms were explored. These findings provide valuable insights into the immune suppression and tumorigenesis caused by ALV-J infection.

Conclusions

The bone marrow microenvironment of chickens with severe ALV-J infection (sample ALV) was in a lower immunocompetence compared with chickens with mild ALV-J infection, which might relate to the increase in double positive T cells and regulatory T cells. Furthermore, our data confirm that cells in the same cluster are differentially susceptible

to ALV-J and that this difference may be related to the activation of "Signaling by Rho Family GTPases". Moreover, our results could contribute to the understanding of bone marrow lymphocytes in different infection states of ALV-J.

Author contributions

Cheng Liu: Writing – original draft, Writing – review and editing, Methodology, Conceptualization, Validation. **Yu Zhang**: Writing – review and editing, Data curation, Conceptualization. **Ruyu Liao**: Writing – review and editing, Formal analysis. **Lecheng Wang**: Writing – review and editing, Visualization. **Xinyi Zhou**: Writing – review and editing, Data curation. **Min Tan**: Writing – review and editing, Data curation. **Zhifu Cui**: Writing – review and editing, Data curation. **Keyun Xu**: Data curation. **Yongju Zhao**: Writing – review and editing, Data curation. **Haiwei Wang**: Writing – review and editing, Data curation. **Qigui Wang**: Writing – review and editing. **Xi Lan**: Writing – review and editing, Project, administration, Funding acquisition, Formal analysis, Supervision.

Ethics statement

All animal experiments were approved by the South West University Animal Ethics Review Committee. All methods are reported in accordance with ARRIVE guidelines (https://arriveguidelines.org) for the reporting of animal experiments. All operations on animals were carried out in accordance with the guidelines established by this committee and the international standards for animal welfare (Project ID: IACUC-20221022-17).

Availability of data and materials

The datasets generated and/or analysed during the current study have been uploaded to the NCBI database under BioProject ID: PRJNA973044.

Funding

This work was financially supported by the Project of Chongqing Agricultural Science Innovation (NW202209), Chongqing Science and Enterprise Consortium Germplasm Resources Collection and Utilization and Variety Trial (KQ202301), Breeding of New Breeds (Synthetic Line) of High-Quality Chickens for Both Meat and Eggs (cstc2021 jscx-gksbX0004), Postdoctoral Research Foundation of China (208155) and the National Natural Science Foundation of China (31802054).

Declaration of interest

The authors declare that they have no known competing financial interests or personal relationships that could have appeared to influence the work reported in this paper.

Acknowledgements

All members of Professor Xi Lan ’s research group at Southwest University.

Supplementary materials

Supplementary material associated with this article can be found, in the online version, at doi:10.1016/j.psj.2025.104995.

References

Ali, A., Vaikari, V.P., Alachkar, H., 2022. CD99 in malignant hematopoiesis. Exp. Hematol. 106, 40–46.

Bassez, A., Vos, H., Van Dyck, L., Floris, G., Arijs, I., Desmedt, C., Boeckx, B., Vanden Bempt, M., Nevelsteen, I., Lambein, K., 2021. A single-cell map of intratumoral changes during anti-PD1 treatment of patients with breast cancer. Nat. Med. 27, 820–832.

Bearer, E.L., Wu, C., 2019. Herpes simplex virus, Alzheimer’s disease and a possible role for rab GTPases. Front. Cell Develop. Biol. 7, 134.

Becht, E., McInnes, L., Healy, J., Dutertre, C.A., Kwok, I.W.H., Ng, L.G., Ginhoux, F., Newell, E.W., 2019. Dimensionality reduction for visualizing single-cell data using UMAP. Nat. Biotechnol. 37, 38-+.

Braga, W.M., Atanackovic, D., Colleoni, G.W., 2012. The role of regulatory T cells and TH17 cells in multiple myeloma. J. Immunol. Res. 2012, 293479.

Burkhardt, N.B., Elleder, D., Schusser, B., Krchlíková, V., Göbel, T.W., Härtle, S., Kaspers, B., 2022. The discovery of chicken foxp3 demands redefinition of avian regulatory T cells. J. Immunol. 208, 1128–1138.

Cai, C., Wan, P., Wang, H., Cai, X., Wang, J., Chai, Z., Wang, J., Wang, H., Zhang, M., Yang, N., 2023. Transcriptional and open chromatin analysis of bovine skeletal muscle development by single-cell sequencing. Cell Proliferat. 56, e13430.

Castellino, F., Huang, A.Y., Altan-Bonnet, G., Stoll, S., Scheinecker, C., Germain, R.N., 2006. Chemokines enhance immunity by guiding naive CD8(+) T cells to sites of CD4 T cell-dendritic cell interaction. Nature 440, 890–895.

Castro, C.D., Flajnik, M.F., 2014. Putting J chain back on the map: how might its expression define plasma cell development? J. Immunol. 193, 3248–3255.

Chen, J., Wang, X., Ma, A., Wang, Q.E., Liu, B., Li, L., Xu, D., Ma, Q., 2022. Deep transfer learning of cancer drug responses by integrating bulk and single-cell RNA-seq data. Nat. Commun. 13, 6494.

Cheng, S.B., Ferland, P., Webster, P., Bearer, E.L., 2011. Herpes simplex virus dances with amyloid precursor protein while exiting the cell. PLoS One 6, e17966.

Chung, W.J., Connick, E., Wodarz, D., 2023. Human immunodeficiency virus (HIV) dynamics in secondary lymphoid tissues and the evolution of cytotoxic T lymphocyte (CTL) escape mutants. bioRxiv, 2023.2003. 2010.532137.

Corradi, G., Bassani, B., Simonetti, G., Sangaletti, S., Vadakekolathu, J., Fontana, M.C., Pazzaglia, M., Gulino, A., Tripodo, C., Cristiano, G., 2022. Release of IFNγ by acute myeloid leukemia cells remodels bone marrow immune microenvironment by inducing regulatory T cells. Clin. Cancer Res. 28, 3141–3155.

Dahlhoff, J., Manz, H., Steinfatt, T., Delgado-Tascon, J., Seebacher, E., Schneider, T., Wilnit, A., Mokhtari, Z., Tabares, P., Böckle, D., 2022. Transient regulatory T-cell targeting triggers immune control of multiple myeloma and prevents disease progression. Leukemia 36, 790–800.

Dai, M., Feng, M., Xie, T., Li, Y., Ruan, Z., Shi, M., Liao, M., Zhang, X., 2017. ALV-J infection induces chicken monocyte death accompanied with the production of IL-1β and IL-18. Oncotarget 8, 99889.

Dai, M., Xu, C., Chen, W., Liao, M., 2019a. Progress on chicken T cell immunity to viruses. Cell. Mol. Life Sci. 76, 2779–2788.

Dai, M., Zhu, S., An, Z., You, B., Li, Z., Yao, Y., Nair, V., Liao, M., 2023. Dissection of key factors correlating with H5N1 avian influenza virus driven inflammatory lung injury of chicken identified by single-cell analysis. PLoS Pathog. 19, e1011685.

Dai, M.M., Xu, C.G., Chen, W.S., Liao, M., 2019b. Progress on chicken T cell immunity to viruses. Cell. Mol. Life Sci. 76, 2779–2788.

Del Pulgar, T.G., Benitah, S.A., Valerón, P.F., Espina, C., Lacal, J.C., 2005. Rho GTPase expression in tumourigenesis: evidence for a significant link. Bioessays 27, 602–613.

Duan, M., Hao, J., Cui, S., Worthley, D.L., Zhang, S., Wang, Z., Shi, J., Liu, L., Wang, X., Ke, A., 2018. Diverse modes of clonal evolution in HBV-related hepatocellular carcinoma revealed by single-cell genome sequencing. Cell Res. 28, 359–373.

Epling-Burnette, P.K., List, A.F., 2009. Advancements in the molecular pathogenesis of myelodysplastic syndrome. Curr. Opin. Hematol. 16, 70–76.

Fang, Z., Li, J., Cao, F., Li, F., 2022. Integration of scRNA-Seq and bulk RNA-seq reveals molecular characterization of the immune microenvironment in acute pancreatitis. Biomolecules 13, 78.

Ge, T., Wen, Y., Li, B., Huang, X., Jiang, S., Zhang, E., 2023. Single-cell sequencing reveals the reproductive variations between primiparous and multiparous Hu ewes. J. Anim. Sci. Biotechnol. 14, 144.

Glenthøj, A., Ørskov, A.D., Hansen, J.W., Hadrup, S.R., O`Connell, C., Grønbæk, K., 2016. Immune mechanisms in myelodysplastic syndrome. Int. J. Mol. Sci. 17, 944.

Grivel, J.C., Penn, M.L., Eckstein, D.A., Schramm, B., Speck, R.F., Abbey, N.W., Herndier, B., Margolis, L., Goldsmith, M.A., 2000. Human immunodeficiency virus type 1 coreceptor preferences determine target T-cell depletion and cellular tropism in human lymphoid tissue. J. Virol. 74, 5347–5351.

Gurung, A., Kamble, N., Kaufer, B.B., Pathan, A., Behboudi, S., 2017. Association of Marek’s disease induced immunosuppression with activation of a novel regulatory T cells in chickens. PLoS Pathog. 13, e1006745.

Haga, R.B., Ridley, A.J., 2016. Rho GTPases: regulation and roles in cancer cell biology. Small GTPases 7, 207–221.

Hawkins, E.D., Duarte, D., Akinduro, O., Khorshed, R.A., Passaro, D., Nowicka, M., Straszkowski, L., Scott, M.K., Rothery, S., Ruivo, N., 2016. T-cell acute leukaemia exhibits dynamic interactions with bone marrow microenvironments. Nature 538, 518–522.

Ho, D.W.H., Tsui, Y.M., Chan, L.K., Sze, K.M.F., Zhang, X., Cheu, J.W.S., Chiu, Y.T., Lee, J.M.F., Chan, A.C.Y., Cheung, E.T.Y., 2021. Single-cell RNA sequencing shows the immunosuppressive landscape and tumor heterogeneity of HBV-associated hepatocellular carcinoma. Nat. Commun. 12, 3684.

Hodge, R.G., Ridley, A.J., 2016. Regulating Rho GTPases and their regulators. Nat. Rev. Mol. Cell Biol. 17, 496–510.

Hohtari, H., Brück, O., Blom, S., Turkki, R., Sinisalo, M., Kovanen, P.E., Kallioniemi, O., Pellinen, T., Porkka, K., Mustjoki, S., 2019. Immune cell constitution in bone marrow microenvironment predicts outcome in adult ALL. Leukemia 33, 1570–1582.

Hu, W., Dong, X., Tian, Z., Zhang, Z., Tang, J., Liang, B., Liu, Q., Chu, M., 2021. Expression, structure and function analysis of the sperm-oocyte fusion genes Juno and Izumo1 in sheep (Ovis aries). J. Anim. Sci. Biotechnol. 12, 1–18.
Isidori, A., Salvestrini, V., Ciciarello, M., Loscocco, F., Visani, G., Parisi, S., Lecciso, M., Ocadlikova, D., Rossi, L., Gabucci, E., 2014. The role of the immunosuppressive microenvironment in acute myeloid leukemia development and treatment. Expert Rev. Hematol. 7, 807–818.
Jansen, S., Gosens, R., Wieland, T., Schmidt, M., 2018. Paving the Rho in cancer metastasis: rho GTPases and beyond. Pharmacol. Therapeut. 183, 1–21.
Ko, S.Y., Barengo, N., Ladanyi, A., Lee, J.S., Marini, F., Lengyel, E., Naora, H., 2012. HOXA9 promotes ovarian cancer growth by stimulating cancer-associated fibroblasts. J. Clin. Investig. 122, 3603–3617.
Koskela, K., Kohonen, P., Salminen, H., Uchida, T., Buerstedde, J.M., Lassila, O., 2004. Identification of a novel cytokine-like transcript differentially expressed in avian γδ T cells. Immunogenetics 55, 845–854.
Krensky, A., Clayberger, C., 2009. Biology and clinical relevance of granulysin. Tissue Antig. 73, 193–198.
Kreslavsky, T., Vilagos, B., Tagoh, H., Poliakova, D.K., Schwickert, T.A., Wöhner, M., Jaritz, M., Weiss, S., Taneja, R., Rossner, M.J., 2017. Essential role for the transcription factor Bhlhe41 in regulating the development, self-renewal and BCR repertoire of B-1a cells. Nat. Immunol. 18, 442–455.
Kuipery, A., Gehring, A.J., Isogawa, M., 2020. Mechanisms of HBV immune evasion. Antiviral Res. 179, 104816.
Lai, H., Zhang, H., Ning, Z., Chen, R., Zhang, W., Qing, A., Xin, C., Yu, K., Cao, W., Liao, M., 2011. Isolation and characterization of emerging subgroup J avian leukosis virus associated with hemangioma in egg-type chickens. Vet. Microbiol. 151, 275–283.
Lamble, A.J., Kosaka, Y., Laderas, T., Maffit, A., Kaempf, A., Brady, L.K., Wang, W., Long, N., Saultz, J.N., Mori, M., 2020. Reversible suppression of T cell function in the bone marrow microenvironment of acute myeloid leukemia. Proc. Natl. Acad. Sci. 117, 14331–14341.
Laparidou, M., Schlickenrieder, A., Thoma, T., Lengyel, K., Schusser, B., 2020. Blocking of the CXCR4-CXCL12 interaction inhibits the migration of chicken B cells into the bursa of Fabricius. Front. Immunol. 10.
Levine, J.H., Simonds, E.F., Bendall, S.C., Davis, K.L., Amir, E.A.D., Tadmor, M.D., Litvin, O., Fienberg, H.G., Jager, A., Zunder, E.R., Finck, R., Gedman, A.L., Radtke, I., Downing, J.R., Pe'er, D., Nolan, G.P., 2015. Data-driven phenotypic dissection of AML reveals progenitor-like cells that correlate with prognosis. Cell 162, 184–197.
Li, J., Xing, S., Zhao, G., Zheng, M., Yang, X., Sun, J., Wen, J., Liu, R., 2020. Identification of diverse cell populations in skeletal muscles and biomarkers for intramuscular fat of chicken by single-cell RNA sequencing. BMC Genom. 21, 1–11.
Li, M.O., Wan, Y.Y., Flavell, R.A., 2007. T cell-produced transforming growth factor-β1 controls T cell tolerance and regulates Th1-and Th17-cell differentiation. Immunity 26, 579–591.
Liu, D., Dai, M., Zhang, X., Cao, W., Liao, M., 2016a. Subgroup J avian leukosis virus infection of chicken dendritic cells induces apoptosis via the aberrant expression of microRNAs. Sci. Rep. 6, 20188.
Liu, D., Qiu, Q., Zhang, X., Dai, M., Qin, J., Hao, J., Liao, M., Cao, W., 2016b. Infection of chicken bone marrow mononuclear cells with subgroup J avian leukosis virus inhibits dendritic cell differentiation and alters cytokine expression. Infect. Genet. Evol. 44, 130–136.
Liu, J., Xu, J., 2020. Regulation of cancer immune checkpoints molecular and cellular mechanisms and therapy introduction. Pages 1-6Springer International Publishing AG Gewerbestrasse 11. CHAM.
Lopes, J.E., Torgerson, T.R., Schubert, L.A., Anover, S.D., Ocheltree, E.L., Ochs, H.D., Ziegler, S.F., 2006. Analysis of FOXP3 reveals multiple domains required for its function as a transcriptional repressor. J. Immunol. 177, 3133–3142.
Matsumoto, Y., Fujita, T., Hirai, I., Sahara, H., Torigoe, T., Ezoe, K., Saito, T., Cruikshank, W.W., Yotsuyanagi, T., Sato, N., 2009. Immunosuppressive effect on T cell activation by interleukin-16-and interleukin-10-cDNA-double-transfected human squamous cell line. Burns 35, 383–389.
McFadden, C., Morgan, R., Rahangdale, S., Green, D., Yamasaki, H., Center, D., Cruikshank, W., 2007. Preferential migration of T regulatory cells induced by IL-16. J. Immunol. 179, 6439–6445.
Medaglia, C., Giladi, A., Stoler-Barak, L., De Giovanni, M., Salame, T.M., Biram, A., David, E., Li, H., Iannacone, M., Shulman, Z., 2017. Spatial reconstruction of immune niches by combining photoactivatable reporters and scRNA-seq. Science 358, 1622–1626.
Mei, Y., Xiao, W., Hu, H., Lu, G., Chen, L., Sun, Z., Lü, M., Ma, W., Jiang, T., Gao, Y., 2021. Single-cell analyses reveal suppressive tumor microenvironment of human colorectal cancer. Clin. Transl. Med. 11, e422.
Merwe, P.A.v.d., Davis, S.J., 2003. Molecular interactions mediating T cell antigen recognition. Ann. Rev. Immunol. 21, 659–684.
Moorthy, R.K., Srinivasan, C., Kannan, M., Arockiam, A.J.V., 2023. Deregulation of MiR-375 inhibits HOXA5 and promotes migration, invasion, and cell proliferation in breast cancer. Appl. Biochem. Biotechnol. 195, 4503–4523.
Okoye, A.A., Picker, L.J., 2013. CD 4+ T-cell depletion in HIV infection: mechanisms of immunological failure. Immunol. Rev. 254, 54–64.
Pai, P., Wang, G., Teo, W.W., Raez-Rodriguez, D., Gabrielson, K.L., Győrffy, B., Downs, B. M., Aggarwal, A., Sukumar, S., 2022. HOXA5-mediated stabilization of iκbα inhibits the NF-κb pathway and suppresses malignant transformation of breast epithelial cells. Cancer Res. 82, 3802–3814.
Pal, A., Pal, A., Mallick, A.I., Biswas, P., Chatterjee, P., 2020. Molecular characterization of Bu-1 and TLR2 gene in Haringhata Black chicken. Genomics 112, 472–483.
Pan, Y., Bi, F., Liu, N., Xue, Y., Yao, X., Zheng, Y., Fan, D., 2004. Expression of seven main Rho family members in gastric carcinoma. Biochem. Biophys. Res. Commun. 315, 686–691.
Pardo, J., Balkow, S., Anel, A., Simon, M.M., 2002. The differential contribution of granzyme A and granzyme B in cytotoxic T lymphocyte-mediated apoptosis is determined by the quality of target cells. Eur. J. Immunol. 32, 1980–1985.
Payne, L., Brown, S., Bumstead, N., Howes, K., Frazier, J.A., Thouless, M.E., 1991. A novel subgroup of exogenous avian leukosis virus in chickens. J. Gen. Virol. 72, 801–807.
Payne, L., Nair, V., 2012. The long view: 40 years of avian leukosis research. Avian Pathol. 41, 11–19.
Potts, N.D., Bichet, C., Merat, L., Guitton, E., Krupa, A.P., Burke, T.A., Kennedy, L.J., Sorci, G., Kaufman, J., 2019. Development and optimization of a hybridization technique to type the classical class I and class II B genes of the chicken MHC. Immunogenetics 71, 647–663.
Qu, X., Li, X., Li, Z., Liao, M., Dai, M., 2022. Chicken peripheral blood mononuclear cells response to Avian Leukosis virus subgroup J infection assessed by single-cell RNA sequencing. Front. Microbiol. 13, 800618.
Quinn, K., Brindley, M.A., Weller, M.L., Kaludov, N., Kondratowicz, A., Hunt, C.L., Sinn, P.L., McCray Jr, P.B., Stein, C.S., Davidson, B.L., 2009. Rho GTPases modulate entry of Ebola virus and vesicular stomatitis virus pseudotyped vectors. J. Virol. 83, 10176–10186.
Rathinam, R., Berrier, A., Alahari, S.K., 2011. Role of Rho GTPases and their regulators in cancer progression. Front. Biosci. 16, 2561–2571.
Richmond, J., Tuzova, M., Cruikshank, W., Center, D., 2014. Regulation of cellular processes by interleukin-16 in homeostasis and cancer. J. Cell. Physiol. 229, 139–147.
Schat, K.A., Xing, Z., 2000. Specific and nonspecific immune responses to Marek's disease virus. Dev. Comp. Immunol. 24, 201–221.
Shannon, P., Markiel, A., Ozier, O., Baliga, N.S., Wang, J.T., Ramage, D., Amin, N., Schwikowski, B., Ideker, T., 2003. Cytoscape: a software environment for integrated models of biomolecular interaction networks. Genome Res. 13, 2498–2504.
Sung, J.A., Lam, S., Garrido, C., Archin, N., Rooney, C.M., Bollard, C.M., Margolis, D.M., 2015. Expanded cytotoxic T-cell lymphocytes target the latent HIV reservoir. J. Infect. Dis. 212, 258–263.
Szklarczyk, D., Franceschini, A., Wyder, S., Forslund, K., Heller, D., Huerta-Cepas, J., Simonovic, M., Roth, A., Santos, A., Tsafou, K.P., Kuhn, M., Bork, P., Jensen, L.J., von Mering, C., 2015. STRING v10: protein-protein interaction networks, integrated over the tree of life. Nucl. Acids Res. 43, D447–D452.
Tai, Y.T., Acharya, C., An, G., Moschetta, M., Zhong, M.Y., Feng, X., Cea, M., Cagnetta, A., Wen, K., van Eenennaam, H., 2016. APRIL and BCMA promote human multiple myeloma growth and immunosuppression in the bone marrow microenvironment. Blood. J. Am. Soc. Hematol. 127, 3225–3236.
Tan, Z., Chen, X., Zuo, J., Fu, S., Wang, H., Wang, J., 2023. Comprehensive analysis of scRNA-seq and bulk RNA-seq reveals dynamic changes in the tumor immune microenvironment of bladder cancer and establishes a prognostic model. J. Transl. Med. 21, 223.
Teft, W.A., Kirchhof, M.G., Madrenas, J., 2006. A molecular perspective of CTLA-4 function. Annu. Rev. Immunol. 24, 65–97.
Theodoratos, A., Whittle, B., Enders, A., Tscharke, D.C., Roots, C.M., Goodnow, C.C., Fahrer, A.M., 2010. Mouse strains with point mutations in TAP1 and TAP2. Immunol. Cell Biol. 88, 72–78.
Trapnell, C., Cacchiarelli, D., Grimsby, J., Pokharel, P., Li, S.Q., Morse, M., Lennon, N.J., Livak, K.J., Mikkelsen, T.S., Rinn, J.L., 2014. The dynamics and regulators of cell fate decisions are revealed by pseudotemporal ordering of single cells. Nat. Biotechnol. 32, 381–U251.
Vega, F.M., Ridley, A.J., 2008. Rho GTPases in cancer cell biology. FEBS Lett. 582, 2093–2101.
Visco, C., Tanasi, I., Quaglia, F.M., Ferrarini, I., Fraenza, C., Krampera, M., 2020a. Oncogenic mutations of MYD88 and CD79B in diffuse large B-cell lymphoma and implications for clinical practice. Cancers 12, 2913.
Visco, C., Tanasi, I., Quaglia, F.M., Ferrarini, I., Fraenza, C., Krampera, M., 2020b. Oncogenic mutations of MYD88 and CD79B in diffuse large B-cell lymphoma and implications for clinical practice. Cancers 12.
Voskoboinik, I., Whisstock, J.C., Trapani, J.A., 2015. Perforin and granzymes: function, dysfunction and human pathology. Nat. Rev. Immunol. 15, 388–400.
Wang, L., Gao, P., Li, C., Liu, Q., Yao, Z., Li, Y., Zhang, X., Sun, J., Simintiras, C., Welborn, M., 2023a. A single-cell atlas of bovine skeletal muscle reveals mechanisms regulating intramuscular adipogenesis and fibrogenesis. J. Cachexia Sarcop. Muscle 14, 2152–2167.
Wang, R., Feng, W., Wang, H., Wang, L., Yang, X., Yang, F., Zhang, Y., Liu, X., Zhang, D., Ren, Q., 2020. Blocking migration of regulatory T cells to leukemic hematopoietic microenvironment delays disease progression in mouse leukemia model. Cancer Lett. 469, 151–161.
Wang, W., Cohen, J.A., Wallrapp, A., Trieu, K.G., Barrios, J., Shao, F., Krishnamoorthy, N., Kuchroo, V.K., Jones, M.R., Fine, A., 2019. Age-related dopaminergic innervation augments T helper 2-type allergic inflammation in the postnatal lung. Immunity 51, 1102-1118. e1107.
Wang, X., Pei, J., Xiong, L., Guo, S., Cao, M., Kang, Y., Ding, Z., La, Y., Liang, C., Yan, P., 2023b. Single-cell RNA sequencing reveals atlas of Yak testis cells. Int. J. Mol. Sci. 24, 7982.
Wittner, J., Schuh, W., 2021. Kruppel-like factor 2 (KLF2) in Immune cell migration. Vaccines 9.
Xiao, G., Deng, A.Q., Liu, H.F., Ge, G.X., Liu, X.L., 2012. Activator protein 1 suppresses antitumor T-cell function via the induction of programmed death 1. In: Proceedings

of the National Academy of Sciences of the United States of America, 109, pp. 15419–15424.
Xiong, N., Fu, Y., Hu, S., Xia, M., Yang, J., 2012. CCR10 and its ligands in regulation of epithelial immunity and diseases. Prot. Cell 3, 571–580.
Xu, B., Dong, W., Yu, C., He, Z., Lv, Y., Sun, Y., Feng, X., Li, N., Lee, L.F., Li, M., 2004. Occurrence of avian leukosis virus subgroup J in commercial layer flocks in China. Avian Pathol. 33, 13–17.
Yang, H., Ma, J., Wan, Z., Wang, Q., Wang, Z., Zhao, J., Wang, F., Zhang, Y., 2021. Characterization of sheep spermatogenesis through single-cell RNA sequencing. FASEB J. 35, e21187.
Ye, S., Xiong, F., He, X., Yuan, Y., Li, D., Ye, D., Shi, L., Lin, Z., Zhao, M., Feng, S., 2023. DNA hypermethylation-induced miR-182 silence targets BCL2 and HOXA9 to facilitate the self-renewal of leukemia stem cell, accelerate acute myeloid leukemia progression, and determine the sensitivity of BCL2 inhibitor venetoclax. Theranostics 13, 77.
Ye, T., Haoyuan, Z., Bei, Z., Kangyong, X., 2021. Exploration of biomarkers in osteoarthritis based on bioinformatics. Medicine 100, e26730.
Yokosuka, T., Kobayashi, W., Takamatsu, M., Sakata-Sogawa, K., Zeng, H., Hashimoto-Tane, A., Yagita, H., Tokunaga, M., Saito, T., 2010. Spatiotemporal basis of CTLA-4 costimulatory molecule-mediated negative regulation of T cell activation. Immunity 33, 326–339.
Yoshimura, A., Muto, G., 2011. TGF-β function in immune suppression. Neg. Co-Recept. Ligands 127–147.